PNAS RESEARCH ARTICLE | NEUROSCIENCE
PSYCHOLOGICAL AND COGNITIVE SCIENCES

Intestinal activating transcription factor 4 regulates stress-related behavioral alterations via paraventricular thalamus in male mice

Feixiang Yuan[a,1], Ziheng Zhou[b,1], Shangming Wu[b], Fuxin Jiao[b], Liang Chen[c], Leilei Fang[c], Hanrui Yin[b], Xiaoming Hu[a], Xiaoxue Jiang[a], Kan Liu[b], Fei Xiao[a], Haizhou Jiang[b], Shanghai Chen[a], Zhanju Liu[c], Yousheng Shu[a], and Feifan Guo[a,2]

Edited by Donald Pfaff, Rockefeller University, New York, NY; received September 12, 2022; accepted March 31, 2023

Chronic stress induces depression- and anxiety-related behaviors, which are common mental disorders accompanied not only by dysfunction of the brain but also of the intestine. Activating transcription factor 4 (ATF4) is a stress-induced gene, and we previously show that it is important for gut functions; however, the contribution of the intestinal ATF4 to stress-related behaviors is not known. Here, we show that chronic stress inhibits the expression of ATF4 in gut epithelial cells. ATF4 overexpression in the colon relieves stress-related behavioral alterations in male mice, as measured by open-field test, elevated plus-maze test, and tail suspension test, whereas intestine-specific ATF4 knockout induces stress-related behavioral alterations in male mice. Furthermore, glutamatergic neurons are inhibited in the paraventricular thalamus (PVT) of two strains of intestinal ATF4-deficient mice, and selective activation of these neurons alleviates stress-related behavioral alterations in intestinal ATF4-deficient mice. The highly expressed gut-secreted peptide trefoil factor 3 (TFF3) is chosen from RNA-Seq data from ATF4 deletion mice and demonstrated decreased in gut epithelial cells, which is directly regulated by ATF4. Injection of TFF3 reverses stress-related behaviors in ATF4 knockout mice, and the beneficial effects of TFF3 are blocked by inhibiting PVT glutamatergic neurons using DREADDs. In summary, this study demonstrates the function of ATF4 in the gut–brain regulation of stress-related behavioral alterations, via TFF3 modulating PVT neural activity. This research provides evidence of gut signals regulating stress-related behavioral alterations and identifies possible drug targets for the treatment of stress-related behavioral disorders.

stress-related behaviors | gut–brain | ATF4 | TFF3 | PVT

Significance

Stress and depression are related to intestinal dysfunction. However, the contribution of the intestinal signals to stress-induced behavioral alterations and its mechanisms are poorly understood. Here, we found that gut epithelial activating transcription factor 4 (ATF4) plays an important role in stress-related behaviors. In mice, intestinal ATF4 deficiency led to reduced peptide trefoil factor 3 levels, which activated paraventricular thalamic glutamatergic neurons to influence stress-related behaviors. These findings highlight the importance of gut signals to the stress-related behavioral alterations and provide possible therapeutic strategies for stress-related behavioral symptoms.

Chronic stress can cause pathological alterations that increase the risk of depression and anxiety (1). Depression is one of the most common mental disorders, which severely limits psychosocial functioning and diminishes the quality of life (2, 3). Depression is characterized by irritable mood, disinterest, loss of concentration, increased suicidal thoughts, along with somatic and cognitive changes (4, 5). It is a heterogeneous and etiologically complex disorder involving genomic and environmental factors such as psychological stress and metabolic dysfunction (6–9). Most research on depression has focused on brain changes such as neurotransmitter imbalances, impaired neurogenesis, declining neuroplasticity, and abnormal neuronal circuitry (7, 10, 11). Based on the discovered mechanisms, there are some antidepressant drugs (12, 13). However, approximately 30% of patients respond inadequately to currently available antidepressants (14). Thus, further exploring the pathogenesis of depression and identifying potential therapeutic targets are imperative.

Depression is not only a mental or brain disorder but also a systemic disease (5, 15). Although mainly affecting the brain, depression is usually accompanied by changes in peripheral systems (15, 16). For example, patients with depression exhibit weight loss/gain, immune system disorders, and altered gut microbiota composition (17–20). The gut is closely associated with depression as irritable bowel syndrome and intestinal inflammation are highly correlated with depression (21, 22). For instance, patients with irritable bowel syndrome had significantly higher levels of anxiety and depression than those of healthy controls (23), and there is a bidirectional association between depression and inflammatory bowel disease (24). The mammalian gut has its own nervous system (enteric nervous system, also called brain-in-the-gut) which can relatively independently respond to external signals (25). Patients with depression often present gut-related dysfunction such as appetite disturbances, metabolic disturbances, functional gastrointestinal disorders, and gut microbiota abnormalities (16, 26, 27). Gut microbiome diversity is strongly associated with stress-related behaviors, including major depressive disorder (28, 29). The microbes could influence the function of epithelial cells and the epithelial cells could send signal to the brain by secretion and nerves (26, 30). Despite the established importance of the gut microbiome for gut–brain communication in regulating

Author contributions: F.Y., Z.Z., and F.G. designed research; F.Y., Z.Z., S.W., F.J., and H.Y. performed research; L.C., L.F., X.H., X.J., K.L., S.C., and Z.L. contributed new reagents/analytic tools; F.Y., Z.Z., S.W., F.J., H.Y., F.X., H.J., Y.S., and F.G. analyzed data; and F.Y. wrote the paper.

The authors declare no competing interest.

This article is a PNAS Direct Submission.

[1]F.Y. and Z.Z. contributed equally to this work.

[2]To whom correspondence may be addressed. Email: ffguo@fudan.edu.cn.

This article contains supporting information online at https://www.pnas.org/lookup/suppl/doi:10.1073/pnas.2215590120/-/DCSupplemental.

Published May 1, 2023.

depression, it remains unclear which intestinal epithelial cell signals regulate the development of depression.

Activating transcription factor 4 (ATF4) is a basic leucine zipper transcription factor expressed in many tissues, including the intestine (31–33). It is involved in the regulation of various physiological processes, including inflammatory responses, amino acid and lipid metabolism, endoplasmic reticulum stress, autophagy, and energy homeostasis (34–36). Dysregulation of ATF4 is associated with various animal models of disorders, including models of liver steatosis, Parkinson's disease, and Alzheimer's disease (37–39). However, its role in stress-related behaviors remains unknown.

We previously found that mice with ATF4 deficiency in intestinal epithelial cells developed spontaneous enterocolitis and showed different microbial composition (increased pathogenic bacteria *Escherichia/Shigella* and *Enterococcus* species, and decreased probiotic bacteria *Lactobacillus* and *Faecalibaculum* species) from control mice (33). As gut function is closely related to depression and stress-related behaviors, we speculated that intestinal ATF4 might also be involved in the pathogenesis of stress-related behaviors. The current study aimed to investigate this possibility and elucidate the underlying mechanisms.

Results

Intestinal ATF4 Levels Are Decreased in Mice Exposed to Chronic Stress and ATF4 Overexpression Alleviates Stress-Related Behaviors. Chronic stress is a fundamental etiological factor in depression (40). To mimic stress-induced behaviors and explore the role of the gut under these conditions, we exposed male C57BL/6 mice to 3 wk of CRS and then performed behavioral assays in order (Fig. 1*A*), followed by killing (41). Stress-related phenotypes in mice with CRS were investigated in open-field test (OFT) by decreased time spent and distance covered in the central region, in the elevated plus-maze test (EPM) by reduced duration and number of entries in the open arms, and in the tail suspension test (TST) by increased immobility time (*SI Appendix*, Fig. S1 *A–C*). Then, we found that under CRS, ATF4 mRNA and protein levels were significantly decreased in intestinal epithelial cells (Fig. 1 *B* and *C*), whereas *Atf4* mRNA expression was unchanged in the liver and lamina mesenterii propria (*SI Appendix*, Fig. S1*D*).

To test whether increased enteric ATF4 expression relieves stress-related behaviors, we injected Cre-dependent AAVs expressing ATF4 (AAV-DIO–ATF4-mCherry) or mCherry (AAV-DIO–mCherry) into the colon of male Villin-Cre mice (Fig. 1*D* and *SI Appendix*, Fig. S1*E*). The efficiency of the ATF4 overexpression was validated by the increased mRNA levels of *Atf4* and its downstream genes *Trb3* and *Ddit4* (*SI Appendix*, Fig. S1*F*). The increased range of *Atf4* gene was low, but the downstream genes *Trb3* and *Ddit* strongly increased. We suspected the results may be due to the negative feedback of downstream target genes to the ATF4, which may lead to the lower increase (42). Four weeks after AAV delivery, we tested stress-related behaviors in order, including OFT, EPM, and TST, in the two groups of mice. Mice overexpressing ATF4 in the colon spent more time and traveled more distance in the center area of the OFT, increased the time and entries into the open arms of the EPM, as well as decreased immobility duration in the TST, compared to control mice (Fig. 1 *E–G* and *SI Appendix*, Fig. S1 *G* and *H*). Then, these mice were exposed to 3 wk of CRS to investigate whether ATF4-overexpressing mice show reduced stress-induced behaviors. Although the time and number of entries in open arms were similar in the EPM between the two groups, the ATF4-overexpressing mice had increased time and distance percentage in the central region in the OFT and decreased immobility time in the TST (Fig. 1 *H–J* and *SI Appendix*, Fig. S1 *I* and *J*). Body weight and food intake were similar in these groups (*SI Appendix*, Fig. S1 *K* and *L*).

Mice with ATF4 Deletion in Intestinal Epithelial Cells Exhibit Stress-Related Behavioral Alterations. To investigate the role of intestinal ATF4 expression in stress-related behaviors, we generated intestinal epithelial cell-specific ATF4 deletion ($ATF4^{\triangle IEC}$) mouse lines by crossing floxed ATF4 ($ATF4^{fl/fl}$) with Villin-Cre mice. According to RT-PCR and western blot analysis, ATF4 levels were decreased in jejunal, ileal, and colonic epithelia, but not in the liver, of $ATF4^{\triangle IEC}$ mice, indicating effective ATF4 deletion (*SI Appendix*, Fig. S2 *A* and *B*). Stress-related behavioral alterations in male $ATF4^{\triangle IEC}$ mice were assessed using the OFT, EPM, and TST (*SI Appendix*, Fig. S2*C*). Surprisingly, $ATF4^{\triangle IEC}$ mice spent shorter time and traveled less distance in the center region in the OFT, spent shorter time in and had fewer entry numbers to the open arms in the EPM, and showed increased immobility duration in the TST (*SI Appendix*, Fig. S2 *D–F*).

To test how intestinal epithelial cell-intrinsic ATF4 expression functions in adult mice and to eliminate potential developmental effects of constitutive deletion, we generated an inducible tamoxifen-dependent intestinal epithelial cell-specific ATF4 knockout mouse model ($ATF4^{\triangle IEC\text{-}IND}$) by crossing floxed ATF4 with Villin-CreER mice in which ATF4 deletion in intestinal epithelial cells could be detected after 5 d of tamoxifen treatment every other day (Fig. 2 *A* and *B*) (43, 44). The behavioral tests were performed at least 10 d after tamoxifen treatment finished. In agreement with the results in male $ATF4^{\triangle IEC}$ mice, male $ATF4^{\triangle IEC\text{-}IND}$ mice spent shorter time and traveled less distance in the center region in the OFT, spent shorter time in and had fewer entry numbers to the open arms in the EPM, showed increased immobility duration in the TST and forced swim test (FST), showed decreased sucrose preference in sucrose preference test (SPT) (Fig. 2 *C–F* and *SI Appendix*, Fig. S3 *A–E*), and showed decreased body weight and unchanged food intake (*SI Appendix*, Fig. S3 *F–H*).

As $ATF4^{\triangle IEC}$ mice have spontaneous gut inflammation (33), which is related to anxiety and depression (45), we next evaluated intestinal inflammation levels of $ATF4^{\triangle IEC\text{-}IND}$ mice. The lengths of the small and large intestines, as well as the morphology of the colon in H&E stainings, were similar for $ATF4^{fl/fl}$ and $ATF4^{\triangle IEC\text{-}IND}$ mice (*SI Appendix*, Fig. S3 *I* and *J*). Moreover, mRNA expression levels of inflammatory cytokines, including interleukin (IL)1β (*Il1b*), IL6 (*Il6*), and tumor necrosis factor α (*Tnfa*), were unchanged after ATF4 deletion (*SI Appendix*, Fig. S3*K*). Therefore, intestinal ATF4 deletion-induced stress-related behavioral alterations may be independent of intestinal inflammation.

Paraventricular Thalamus (PVT) Glutamatergic Neurons Mediate Stress-Related Behaviors Caused by Intestinal ATF4 Deletion. As stress-related and depressive-like behaviors are usually accompanied with functional changes of neurons, and gut–brain axis has been closely related to neuronal activity (7, 46), we assumed that intestinal ATF4 deletion may influence neural activity. To investigate changes in brain regions of mice with intestinal ATF4 deletion, we conducted immunofluorescence (IF) stainings to examine changes in basal c-Fos expression, a signal reflecting neuronal activity (47), in embryonic and inducible intestinal ATF4 knockout mice. The c-Fos expression decreased in the paraventricular hypothalamic nucleus (PVN) and PVT and increased in the basolateral amygdala (BLA) of $ATF4^{\triangle IEC}$ mice (*SI Appendix*, Fig. S4 *A* and *B*). While in $ATF4^{\triangle IEC\text{-}IND}$ mice, the c-Fos levels decreased in PVT and BLA, but unchanged in PVN (Fig. 3*A* and *SI Appendix*, Fig. S4*C*). Because c-Fos changes of PVT

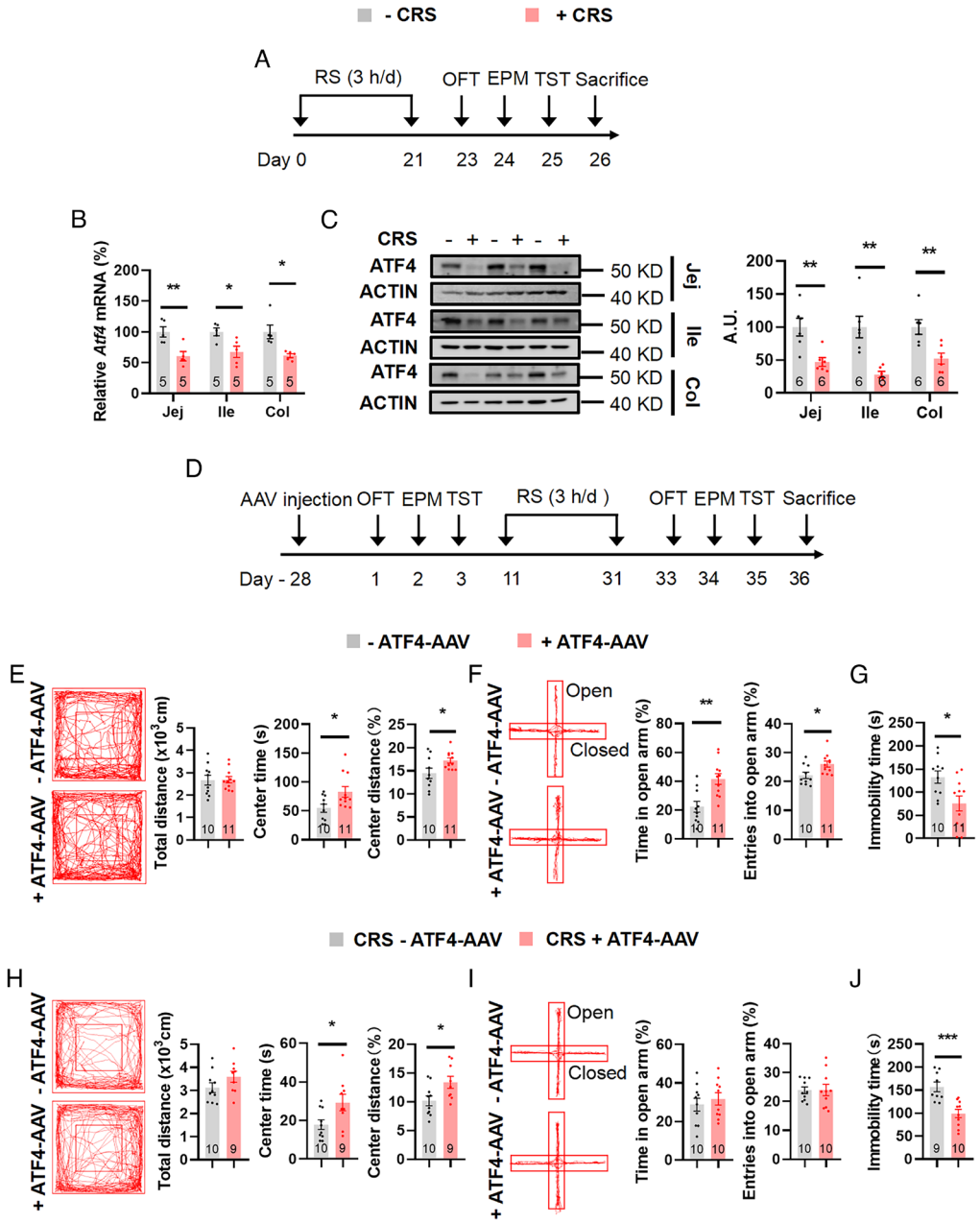

Fig. 1. Colonic epithelial ATF4 overexpression exhibits beneficial behavioral effects under CRS. (*A*) Timeline of the restraint (+CRS) or control (−CRS) protocol and behavioral tests. RS, restraint stress, OFT, open-field test; EPM, elevated plus-maze test; TST, tail suspension test. (*B*) Gene expression of *Atf4* in jejunal (Jej) (t_8 = 3.531, P = 0.0077), ileal (Ile) (t_8 = 2.926, P = 0.0191) and colonic (Col) (Mann–Whitney U test, P = 0.0079) epithelial cells by RT-PCR. (*C*) ATF4 protein in jejunal (t_{10} = 3.526, P = 0.0055), ileal ($t_{5.852}$ = 4.179, P = 0.0061), and colonic (t_{10} = 3.414, P = 0.0066) epithelial cells by western blotting (*Left*) and quantified by densitometric analysis (*Right*), A.U.: arbitrary units. (*D*) Timeline of the adeno-associated virus (AAV) injection, restraint (CRS) protocol, and behavioral tests. (*E* and *H*) Representative tracks of mice in OFT, travel distance (*E*: t_{19} = 0.0771, P = 0.9394; *H*: t_{17} = 1.488, P = 0.1550), time spent in center (*E*: t_{19} = 2.425, P = 0.0255; *H*: t_{17} = 2.367, P = 0.0301), and percentage of distance in center area (*E*: t_{19} = 2.251, P = 0.0364; *H*: t_{17} = 2.400, P = 0.0281). (*F* and *I*) Representative tracks of mice in EPM, percentage of time spent in the open arms (*F*: t_{19} = 3.596, P = 0.0019; *I*: t_{18} = 0.6447, P = 0.5272), and percentage of entries into the open arms (*F*: t_{19} = 2.529, P = 0.0204; *I*: t_{18} = 0.02775, P = 0.9782). (*G* and *J*) Immobility time of TST (*G*: t_{19} = 2.684, P = 0.0147; *J*: t_{17} = 4.204, P = 0.0006). Studies for *A–C* were conducted using 8 to 9-wk-old male wild-type mice with or without CRS; studies for *D–J* were conducted using 8 to 9-wk-old male Villin-Cre mice receiving colonic injection of AAVs expressing mCherry (−AAV–ATF4) or ATF4 (+AAV–ATF4) under normal states (*E–G*) or CRS (*H–J*). Data are expressed as the mean ± SEM (the number of samples is indicated in the bar graph), with individual data points. Data were analyzed via two-tailed unpaired Student's *t* test or specific test marked in the data. *P < 0.05, **P < 0.01, ***P < 0.001.

were consistent in both strains of mice and PVT was closely related with stress-related behaviors (48–50), we focused on this region in subsequent studies. As PVT neurons are primarily glutamatergic neurons (51), we costained the PVT of intestinal ATF4 knockout mice for c-Fos and the marker of synapses receiving glutamatergic terminals, alpha isoform of Ca^{2+}/calmodulin-dependent protein kinase II (CAMKIIα) (52). C-Fos expression in glutamatergic neurons was reduced in the PVT of ATF4$^{\Delta IEC}$ mice (*SI Appendix*, Fig. S4*D*) and ATF4$^{\Delta IEC\text{-}IND}$ mice (Fig. 3*B*).

We also tested whether inhibition of PVT glutamatergic neurons is sufficient to induce depression-like behaviors by injecting inhibitory hM4Di designer receptors exclusively activated by designer drugs (DREADDs) under the CaMKIIα promoter activated by the inert ligand clozapine N oxide (CNO) (51). For this purpose, AAVs with CaMKIIα promoter encoding hM4Di (AAV-CaMKIIα–hM4Di-mCherry) or mCherry alone (AAV-CaMKIIα–mCherry) were injected into the PVT of wild-type mice (*SI Appendix*, Fig. S5 *A* and *B*). The inhibited activity of

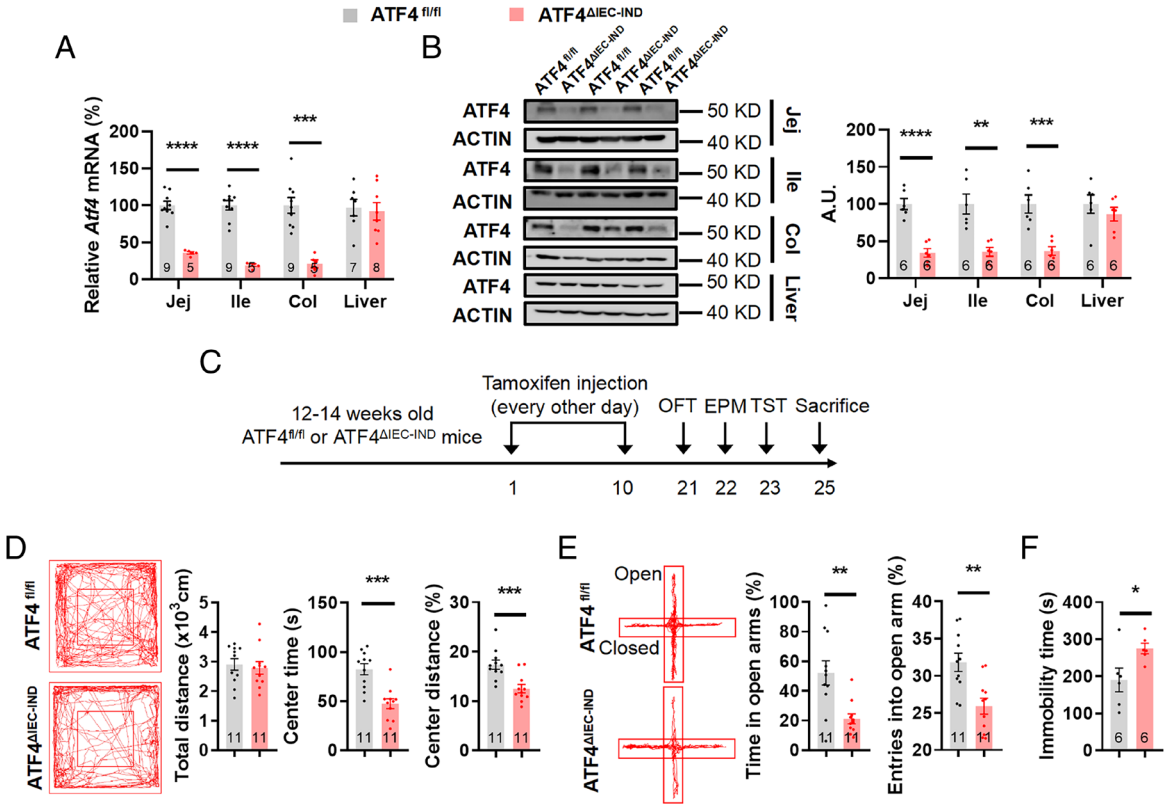

Fig. 2. Inducible intestinal ATF4 knockout mice exhibit stress-related behaviors. (*A*) Gene expression of *Atf4* in jejunal (Jej) (unpaired *t* test with Welch's correction, $t_{9.285} = 11.04$, $P < 0.0001$), ileal (Ile) (unpaired *t* test with Welch's correction, $t_{9.174} = 12.24$, $P < 0.0001$), and colonic (Col) ($t_{12} = 5.288$, $P = 0.0002$) epithelial cells and liver ($t_{13} = 0.3067$, $P = 0.7639$) by RT-PCR. (*B*) ATF4 protein in jejunal ($t_{10} = 6.996$, $P < 0.0001$), ileal ($t_{10} = 4.398$, $P = 0.0013$), and colonic ($t_{10} = 4.709$, $P = 0.0008$) epithelial cells and liver ($t_{10} = 0.8801$, $P = 0.3995$) by western blotting (*Left*) and quantified by densitometric analysis (*Right*), A.U.: arbitrary units. (*C*) Timeline of the tamoxifen injection and behavioral tests in ATF4$^{fl/fl}$ or ATF4$^{\Delta IEC-IND}$ mice. OFT, open-field test; EPM, elevated plus-maze test; TST, tail suspension test. (*D*) Representative tracks of mice in OFT, travel distance ($t_{20} = 0.4083$, $P = 0.6874$), time spent in center ($t_{20} = 4.647$, $P = 0.0002$), and percentage of distance in center area ($t_{20} = 3.867$, $P = 0.001$). (*E*) Representative tracks of mice in EPM, percentage of time spent in the open arms (unpaired *t* test with Welch's correction, $t_{13.28} = 3.519$, $P = 0.0037$), and percentage of entries into the open arms ($t_{20} = 3.617$, $P = 0.0017$). (*F*) Immobility time of TST ($t_{10} = 2.409$, $P = 0.0367$). Studies were conducted using 14 to 16-wk-old male ATF4$^{fl/fl}$ or ATF4$^{\Delta IEC-IND}$ mice. Data are expressed as the mean ± SEM (the number of samples is indicated in the bar graph), with individual data points. Data were analyzed via two-tailed unpaired Student's *t* test or specific test marked in the data. *$P < 0.05$, **$P < 0.01$, ***$P < 0.001$, ****$P < 0.0001$.

PVT glutamatergic neurons was confirmed by decreased c-Fos staining in glutamatergic neurons (reflected by mCherry) of hM4Di-expressing mice (*SI Appendix*, Fig. S5*C*), and 30 min after CNO injection, mice with reduced activity of PVT glutamatergic neurons showed shorter time and less distance in the center region in the OFT, shorter time in and fewer entries to the open arms in the EPM, and increased immobility time in the TST (*SI Appendix*, Fig. S5 *D–F*).

Next, we investigated whether PVT neurons mediate stress-related behavioral alterations induced by gut ATF4 deficiency. To this end, AAVs encoding hM3Dq (AAV-CaMKIIα–hM3Dq-mCherry) or mCherry alone (AAV-CaMKIIα–mCherry) under CaMKIIα promoter control were injected into the PVT of tamoxifen-treated ATF4$^{fl/fl}$ and ATF4$^{\Delta IEC-IND}$ mice (*SI Appendix*, Fig. S6*A*), with i.p. CNO injection 4 wk after AAV delivery. Higher PVT glutamatergic neuronal activity was then confirmed by increased c-Fos staining of glutamatergic neurons (reflected by mCherry) in ATF4$^{fl/fl}$ and hM3Dq-expressing ATF4$^{\Delta IEC-IND}$ mice (*SI Appendix*, Fig. S6*B*). Activation of PVT excitatory neurons by injecting CNO into ATF4$^{\Delta IEC-IND}$ mice resulted in increased center time in the OFT, increased residence time in the open arms in the EPM, and reduced immobility time in the TST (Fig. 3 *C–F* and *SI Appendix*, Fig. S6 *C–F*).

To further confirm the role of PVT glutamatergic neurons in stress-related behavioral alterations, we next explored the function of these neurons in the CRS model. After chronic stress, the number of c-Fos-positive neurons was significantly decreased in the PVT (*SI Appendix*, Fig. S7*A*). To test the effects of chemogenetic activation of PVT glutamatergic neurons on stress-related behavioral alterations, AAVs encoding hM3Dq (AAV-CaMKIIα–hM3Dq-mCherry) or mCherry alone (AAV-CaMKIIα–mCherry) under CaMKIIα promoter control were injected into the PVT of wild-type mice that were subjected to CRS and CNO injection 4 wk afterward. Activation of PVT glutamatergic neural activity was confirmed and improved chronic stress-induced behavioral alterations in OFT, EPM, and TST (*SI Appendix*, Fig. S7 *B–F*). However, activation of PVT glutamatergic neural activity in nonstressed mice had similar behaviors with control mice in OFT and EPM, but showed decreased immobility time in TST (*SI Appendix*, Fig. S8).

Gut TFF3 Mediates Depression-Like Behaviors Induced by Intestinal ATF4 Deletion. Next, we investigated how gut ATF4 expression modulates PVT neuronal activity. As intestinal peptides are important elements of the gut–brain axis (26), we hypothesized that ATF4 may impact secretory peptides that act on the brain. RNA-Seq analysis was performed using ileal epithelial cells of ATF4$^{fl/fl}$ and ATF4$^{\Delta IEC}$ mice (53). To identify secreted proteins that may act on the brain, we crossanalyzed data of differentially expressed genes with data of annotated gut-secreted peptides, which have correlation in functioning on gut–brain signals (54) (Fig. 4*A*). Among several candidate genes with significance of the correlation and high levels verified in the colon and ileum of ATF4$^{\Delta IEC-IND}$ mice (*SI Appendix*, Fig. S9 *A–D* and Fig. 4*B*), only trefoil factor 3 (*Tff3*) and *Ace2* decreased

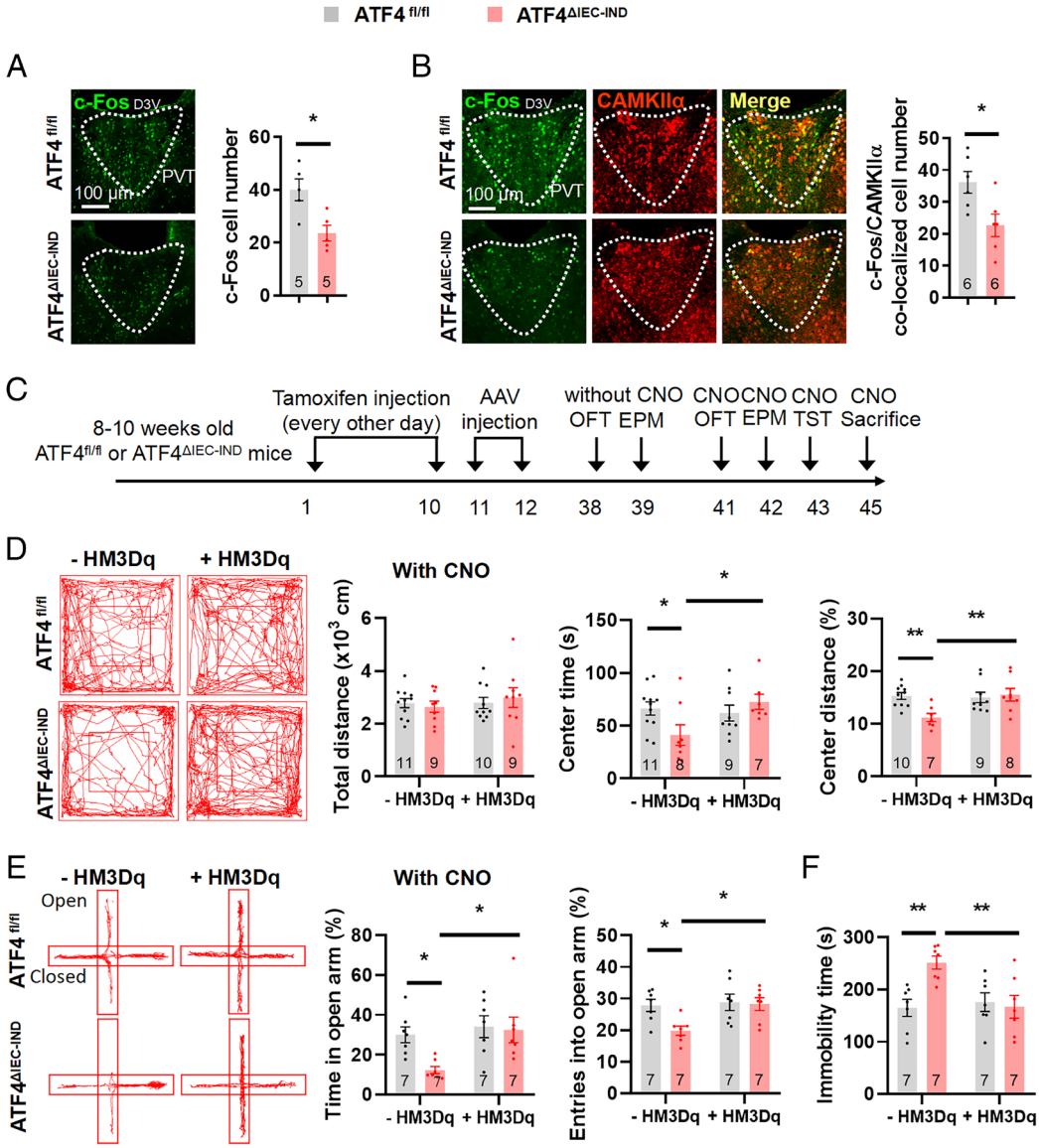

Fig. 3. PVT glutamatergic neuron activation relieves intestinal ATF4 deletion caused stress-related behaviors. (*A*) IF staining for c-Fos (green) in the PVT (*Left*) and quantification of c-Fos cell numbers (*Right*) (t_8 = 3.213, P = 0.0124); D3V, dorsal 3rd ventricle. (*B*) IF staining for c-Fos (green), CAMKIIα (red), or merge (yellow) in the PVT (*Left*), and quantification of c-Fos and CAMKIIα colocalized cell numbers (*Right*) (t_{10} = 2.748, P = 0.0206). (*C*) Timeline of the tamoxifen injection, adeno-associated virus (AAV) injection, and behavioral tests in ATF4$^{fl/fl}$ or ATF4$^{\Delta IEC-IND}$ mice. OFT, open-field test; EPM, elevated plus-maze test; TST, tail suspension test. (*D*) Representative tracks of mice in OFT, travel distance (Genotype Factor: $F_{1,35}$ = 0.01699, P = 0.8970; HM3Dq factor: $F_{1,35}$ = 0.5218, P = 0.4749; Genotype × HM3Dq: $F_{1,35}$ = 0.4704, P = 0.4973), time spent in center (Genotype Factor: $F_{1,31}$ = 0.885, P = 3540; HM3Dq factor: $F_{1,31}$ = 3.067, P = 0.0898; Genotype × HM3Dq: $F_{1,31}$ = 5.286, P = 0.0284), and percentage of distance in center area (Genotype Factor: $F_{1,30}$ = 3.866, P = 0.0586; HM3Dq factor: $F_{1,30}$ = 4.824, P = 0.0359; Genotype × HM3Dq: $F_{1,30}$ = 6.279, P = 0.0179). (*E*) Representative tracks of mice in EPM, percentage of time spent in the open arms (Genotype Factor: $F_{1,24}$ = 4.114, P = 0.0538; HM3Dq factor: $F_{1,24}$ = 6.458, P = 0.0179; Genotype × HM3Dq: $F_{1,24}$ = 2.875, P = 0.1029), and percentage of entries into the open arms (Genotype Factor: $F_{1,24}$ = 4.435, P = 0.0459; HM3Dq factor: $F_{1,24}$ = 5.363, P = 0.0294; Genotype × HM3Dq: $F_{1,24}$ = 3.373, P = 0.0787). (*F*) Immobility time of TST (Genotype Factor: $F_{1,24}$ = 5.006, P = 0.0348; HM3Dq factor: $F_{1,24}$ = 4.436, P = 0.0458; Genotype × HM3Dq: $F_{1,24}$ = 7.477, P = 0.0116). Studies for *A* and *B* were conducted using 14 to 16-wk-old male ATF4$^{fl/fl}$ or ATF4$^{\Delta IEC-IND}$ mice; studies for *C*–*F* were conducted using 10 to 12-wk-old male ATF4$^{fl/fl}$ or ATF4$^{\Delta IEC-IND}$ mice receiving AAVs expressing mCherry (−HM3Dq) or HM3Dq (+HM3Dq), followed by CNO injection. Data are expressed as the mean ± SEM (the number of samples is indicated in the bar graph), with individual data points. Data were analyzed via two-tailed unpaired Student's *t* test for *A* and *B*, or via the two-way ANOVA for *D*–*F*. *P < 0.05, **P < 0.01.

in both segments of the gut. As TFF3 is a mainly gut-derived peptide with reported antidepressant effects (55), we chose this factor in the subsequent studies. The *Tff3* mRNA expression was markedly down-regulated in the intestinal epithelial cells of the jejunum, ileum, and colon following ATF4 ablation (Fig. 4*B* and *SI Appendix*, Fig. S11*A*).

Next, we examined whether ATF4 directly regulates TFF3. ATF4-overexpressing adenoviruses (Ad-ATF4) in CCD-841 cells increased *Tff3* mRNA levels (*SI Appendix*, Fig. S10*A*). Conversely, inhibiting ATF4 with adenoviruses expressing dominant-negative ATF4 (Ad-DN-ATF4) decreased the *Tff3* expression (*SI Appendix*, Fig. S10*B*). As ATF4 regulates the expression of downstream target genes via direct binding to cAMP-responsive element sites in their promoters (56), we hypothesized that ATF4 regulates TFF3 by binding on its promoter. First, we predicted cAMP-responsive element binding sites of the *Tff3* promoter using the bioinformatics tool JASPAR database and identified three sites (*SI Appendix*, Fig. S10*C*). Then, we generated a luciferase reporter plasmid of *Tff3* (pGL3-TFF3), carrying 2,000 bp upstream of the transcription start site in a luciferase reporter vector (pGL3-Basic). The *Tff3* promoter activity was increased by ATF4 overexpression (*SI Appendix*, Fig. S10*C*). These results showed that ATF4 promotes *Tff3* expression directly.

Then, we examined whether intestinal TFF3 could influence TFF3 levels in the serum or brain of intestinal ATF4 knockout mice. The TFF3 levels were reduced in the serum, CSF, and PVT of intestinal epithelial cell-specific ATF4 knockout mice (Fig. 4 *C–E* and *SI Appendix*, Fig. S11 *B–D*). Conversely, serum TFF3 levels were increased in colonic ATF4-overexpressing mice (*SI Appendix*, Fig. S11*E*). As TFF3 is also expressed in the brain (57), we examined *Tff3* mRNA levels in the hypothalamus and PVT and the gene expression was comparable in control and ATF4-ablated mice (*SI Appendix*, Fig. S11 *F* and *G*). To further confirm that TFF3 can be secreted by intestinal cells following changes in ATF4 expression, we determined TFF3 levels in the culture medium of ATF4-overexpressing CCD-841 cells. The extracellular TFF3 concentration was increased in Ad-ATF4-treated cultures (*SI Appendix*, Fig. S11*H*).

As TFF3 levels were decreased in the serum and CSF of mice with intestinal epithelial cell-specific ATF4 deletion and TFF3 is closely associated with depressive behaviors (55, 58), we presumed that TFF3 mediates stress-related behaviors caused by ATF4 knockout. We i.p. injected TFF3 into ATF4$^{\triangle IEC\text{-}IND}$ mice (Fig. 4 *F* and *G*). As expected, the changed behavioral alterations in ATF4$^{\triangle IEC\text{-}IND}$ mice were alleviated by TFF3 injection (Fig. 4 *H–J* and *SI Appendix*, Fig. S11 *I* and *J*), carried out in different groups of mice.

As the protein levels of TFF3 were decreased in the PVT of ATF4$^{\triangle IEC\text{-}IND}$ mice, these behavioral TFF3 effects might be mediated by PVT neurons. To study the roles of TFF3 in the PVT, we injected TFF3 into the PVT of ATF4$^{\triangle IEC\text{-}IND}$ mice (Fig. 5 *A* and *B* and *SI Appendix*, Fig. S12*A*). After TFF3 injection, TFF3 levels in the PVT of ATF4$^{\triangle IEC\text{-}IND}$ mice returned to normal values (Fig. 5*C*), and these mice showed increased center time in the OFT, increased open arm time in the EPM, and reduced immobility time in the TST compared to those without TFF3 treatment (Fig. 5 *D–F* and *SI Appendix*, Fig. S12 *B* and *C*). To further confirm the role of TFF3 in the PVT, we injected TFF3 in the PVT in wild-type mice (*SI Appendix*, Fig. S13 *A* and *B*). The TFF3 levels increased in the PVT but not in the hypothalamus or cortex (*SI Appendix*, Fig. S13 *C* and *D*). PVT injection of TFF3 in wild-type mice also exhibited increased center time and distance in OFT, increased time and entries in the open arms of EPM, and reduced immobility time in TST (*SI Appendix*, Fig. S13 *E–G*).

TFF3 Stimulates PVT Neural Activity Facilitating Antidepressant Effects in ATF4$^{\triangle IEC\text{-}IND}$ Mice. As previous studies reported that TFF3 activates neural activity, we hypothesized that TFF3 may stimulate PVT neurons. We treated primary thalamic neurons with different concentrations of TFF3 peptides and found increased *Fos* mRNA and c-Fos protein levels after TFF3 treatment (*SI Appendix*, Fig. S14 *A* and *B*). Furthermore, IF c-Fos stainings showed that ATF4$^{\triangle IEC\text{-}IND}$ mice treated with TFF3 had increased c-Fos expression compared to ATF4$^{\triangle IEC\text{-}IND}$ mice treated with saline (Fig. 6*A*). To investigate whether beneficial TFF3 effects were mediated by PVT neural activity, we inhibited this activity in TFF3-treated ATF4$^{\triangle IEC\text{-}IND}$ mice (Fig. 6*B* and *SI Appendix*, Fig. S15*A*) using an inhibitory hM4Di DREADD. To this end, AAVs encoding hM4Di (AAV-CaMKIIα–hM4Di-mCherry) or mCherry alone (AAV-CaMKIIα–mCherry) under CaMKIIα promoter control were injected into the PVT of ATF4$^{fl/fl}$ or ATF4$^{\triangle IEC\text{-}IND}$ mice, and these mice were subjected to i.p. injection of saline or TFF3, as well as CNO injection, 4 wk after AAV delivery. The TFF3-induced stimulation in ATF4$^{\triangle IEC\text{-}IND}$ mice and the hM4Di-induced inhibition of PVT glutamatergic neuronal activity in TFF3-treated ATF4$^{\triangle IEC\text{-}IND}$ mice were then confirmed by respective increases and decreases in c-Fos stainings of glutamatergic neurons (reflected by mCherry; *SI Appendix*, Fig. S15*B*). In behavioral experiments, beneficial TFF3 effects in ATF4$^{\triangle IEC\text{-}IND}$ mice were blocked by inhibiting PVT glutamatergic neuronal activity, as confirmed by the OFT, EPM, and TST (Fig. 6 *C–E* and *SI Appendix*, Fig. S15 *C* and *D*). Intraperitoneal injection of TFF3 in wild-type mice had no behavioral alterations in OFT or EPM, but reduced immobility time in TST (*SI Appendix*, Fig. S16). Simply, inhibition of PVT glutamatergic neurons exhibited reduced center time and distance in OFT, reduced time and entries in the open arms of EPM, and increased immobility time in TST in ATF4$^{fl/fl}$ mice, but had no obvious changes in ATF4$^{\triangle IEC\text{-}IND}$ mice (*SI Appendix*, Fig. S17).

Discussion

Depression is a common mental disorder, a leading cause of disability worldwide, and a major contributor to the overall global disease burden (2). Depression results from a complex interaction of social stress, psychological stress, and biological factors (8). Gut dysfunction is closely related to stress-related depression-associated behavioral alterations (59, 60). This study found that the intestinal epithelial signal ATF4 was reduced in chronic restraint stressed male mouse models and contributed to the development of stress-related behavioral alterations. Mechanistically, gut ATF4 regulated the expression of the gut-secreted peptide TFF3, which activated PVT glutamatergic neurons to induce beneficial behavioral effects (Fig. 6*F*). As all the experiments were performed in male mice, we did not know whether female mice also exhibit similar behaviors and mechanisms, since sex differences are important for behavioral tests and should not be overlooked (48). It requires further study.

ATF4 is a stress response protein that can induce the transcription of various genes under certain conditions, including endoplasmic reticulum stress, amino acid deprivation, and hypoxia (34). However, the ATF4 response to chronic stress remains limited, and we do not know why intestinal epithelial cell-specific ATF4 expression is decreased under CRS. A possible mechanism is that microRNA (miR)-214 levels change in some stress conditions and pre-miR-214 overexpression inhibits ATF4 expression (61, 62). Other studies report that asparagine levels are increased in depression models and decreased following antidepressant treatment, which may inhibit ATF4 expression (63–65). How chronic stress inhibits ATF4 expression requires further research.

Intestinal epithelial cells secrete many peptides that enter the bloodstream and act on target organs (26, 66). TFF3 is a peptide mainly secreted by intestinal goblet cells (67). It protects the intestinal mucosa from various injuries and facilitates mucosal restitution by promoting cell migration and inhibiting apoptosis (68, 69). TFF3 is also expressed in the liver, pancreas, and brain (57, 70, 71). Intracerebral and i.p. injections of TFF3 have antidepressant effects (55, 72). However, the function of gut-derived TFF3 remains unknown. Our study demonstrated that ATF4 deletion in gut resulted in reduced serum TFF3 levels and colon-specific ATF4 overexpression induced increased TFF3 serum concentrations, implying that gut ATF4–TFF3 expression contributes to blood TFF3 levels. Moreover, ATF4 upregulation in CCD-841 cells influenced TFF3 levels in cell culture mediums. However, we cannot exclude contributions from other organs or tissues. For example, we did not examine the TFF3 expression in other brain regions or immune cells, and the serum TFF3 may change because of other tissues. These possibilities need further exploration.

Recently, the gut–brain axis has attracted a lot of attention. The gut can influence brain function in various ways such as secreted peptides, gut microbiota, and vagus and enteric nerves (25, 73). In the present study, gut microbiota may have participated in the

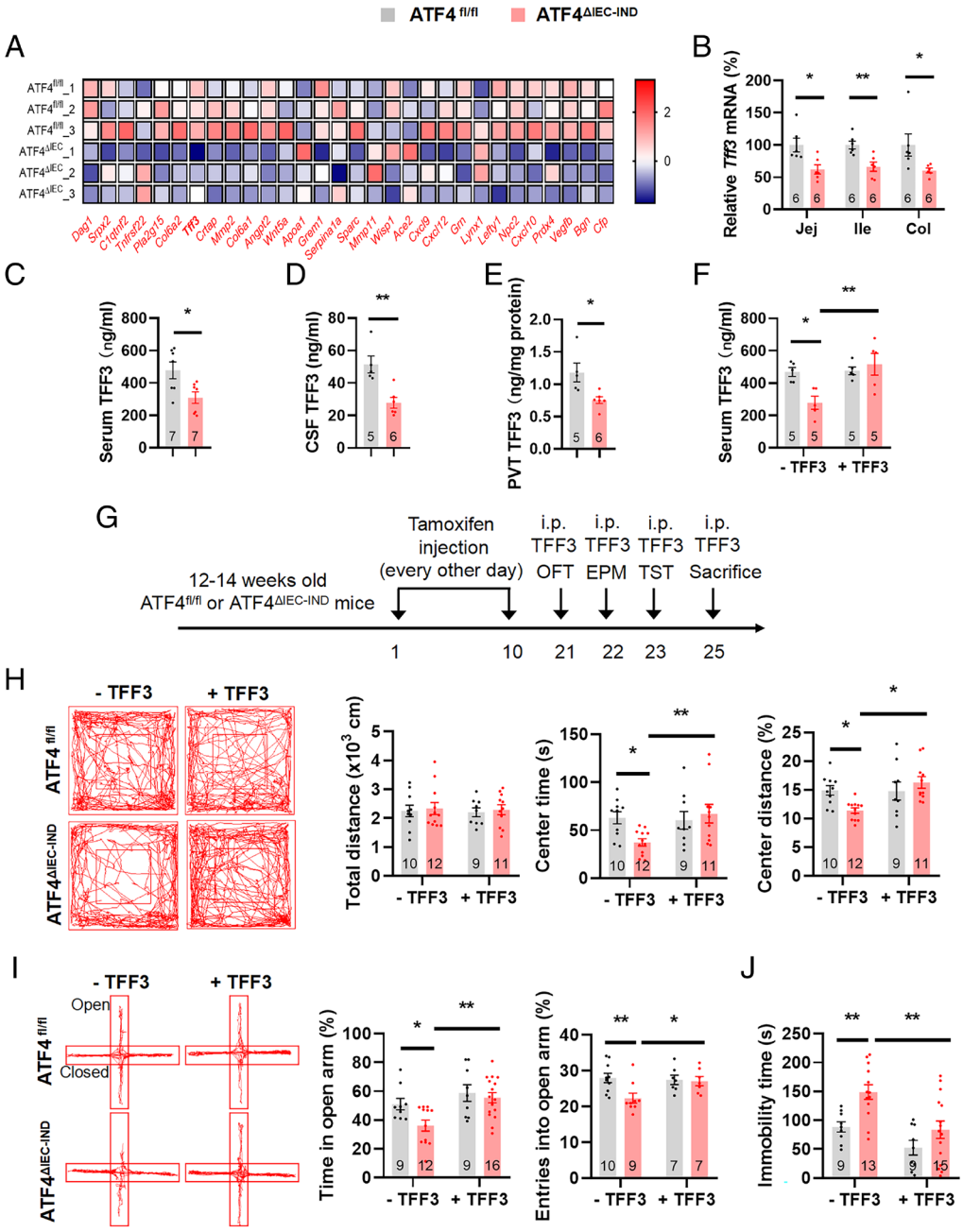

Fig. 4. TFF3 administration relieves intestinal ATF4 deletion caused stress-related behaviors. (*A*) Heatmap showing differentially expressed gut-secreted genes in ileac epithelial cells from ATF4$^{fl/fl}$ and ATF4$^{\triangle IEC}$ mice. (*B*) Gene expression of Tff3 in jejunal (Jej) (t_{10} = 2.968, P = 0.0141), ileal (Ile) (t_{10} = 3.591, P = 0.0049), and colonic (Col) (Mann–Whitney U test, P = 0.0087) epithelial cells by RT-PCR. (*C*) TFF3 levels in serum by ELISA (t_{12} = 2.692, P = 0.0196, CV of ATF4$^{fl/fl}$: 28.58%, CV of ATF4$^{\triangle IEC-IND}$: 30.50%). (*D*) TFF3 levels in cerebrospinal fluid (CSF) by ELISA (t_9 = 3.941, P = 0.0034, CV of ATF4$^{fl/fl}$: 22.78%, CV of ATF4$^{\triangle IEC-IND}$: 29.48%). (*E*) TFF3 levels in PVT by ELISA (t_9 = 2.945, P = 0.0164, CV of ATF4$^{fl/fl}$: 27.89%, CV of ATF4$^{\triangle IEC-IND}$: 16.93%). (*F*) TFF3 levels in serum by ELISA (Genotype Factor: $F_{1,16}$ = 3.068, P = 0.0990; TFF3 factor: $F_{1,16}$ =8.243, P = 0.0111; Genotype × TFF3: $F_{1,16}$ = 7.311, P = 0.0156; CV of ATF4$^{fl/fl}$: 11.35%, CV of ATF4$^{\triangle IEC-IND}$: 42.95%). (*G*) Timeline of the tamoxifen injection, TFF3 i.p. injection, and behavioral tests in ATF4$^{fl/fl}$ or ATF4$^{\triangle IEC-IND}$ mice. OFT, open-field test; EPM, elevated plus-maze test; TST, tail suspension test. (*H*) Representative tracks of mice in OFT, travel distance (Genotype Factor: $F_{1,38}$ = 0.2085, P = 0.6505; TFF3 factor: $F_{1,38}$ = 0.05511, P = 0.8157; Genotype × TFF3: $F_{1,38}$ = 6.033e-005, P = 0.9938), time spent in center (Genotype Factor: $F_{1,38}$ = 1.595, P = 0.2144; TFF3 factor: $F_{1,38}$ = 3.336, P = 0.0756; Genotype × TFF3: $F_{1,38}$ = 4.781, P = 0.0350), and percentage of distance in center area (Genotype Factor: $F_{1,38}$ = 1.044, P = 0.3133; TFF3 factor: $F_{1,38}$ = 5.912, P = 0.0199; Genotype × TFF3: $F_{1,38}$ = 6.511, P = 0.0149). (*I*) Representative tracks of mice in EPM, percentage of time spent in the open arms (Genotype Factor: $F_{1,42}$ = 4.330, P = 0.0436; TFF3 factor: $F_{1,42}$ = 9.751, P = 0.0032; Genotype × TFF3: $F_{1,42}$ = 1.801, P = 0.1868), and percentage of entries into the open arms (Genotype Factor: $F_{1,29}$ = 4.784, P = 0.0369; TFF3 factor: $F_{1,29}$ = 2.426, P = 0.1302; Genotype × TFF3: $F_{1,29}$ = 3.737, P = 0.0630). (*J*) Immobility time of TST (Genotype Factor: $F_{1,42}$ = 10.73, P = 0.0021; TFF3 factor: $F_{1,42}$ = 13.03, P = 0.0008; Genotype × TFF3: $F_{1,42}$ = 1.091, P = 0.3022). Studies for *A* were conducted using 3 to 5-wk-old male ATF4$^{fl/fl}$ or ATF4$^{\triangle IEC}$ mice; studies for *B–E* were conducted using 14 to 16-wk-old male ATF4$^{fl/fl}$ or ATF4$^{\triangle IEC-IND}$ mice; studies for *F–J* were conducted using 14 to 16-wk-old male ATF4$^{fl/fl}$ or ATF4$^{\triangle IEC-IND}$ mice receiving i.p. injection of saline (−TFF3) or TFF3 (+TFF3); and studies for H were conducted using separate groups of mice with same treatments of *F*, *G*, *I*, and *J*. Data are expressed as the mean ± SEM (the number of samples is indicated in the bar graph), with individual data points. Data were analyzed via two-tailed unpaired Student's t test for *B–E*, or via the two-way ANOVA for *F–J*, or specific test marked in the data. *P < 0.05, **P < 0.01.

regulation of stress-related behaviors, as the composition of bacteria changes in mice with intestinal-specific ATF4 deletion (33). Furthermore, intestinal epithelial cell-specific ATF4 may impact brain function via peripheral neurons. For example, ATF4 is a crucial signal for nutrition sensing, and the gut can detect glucose and fat, signals that are transmitted via vagal or spinal afferences to hypothalamic agouti-related peptide (AgRP) neurons (74, 75). Confirmation of these hypotheses requires additional work.

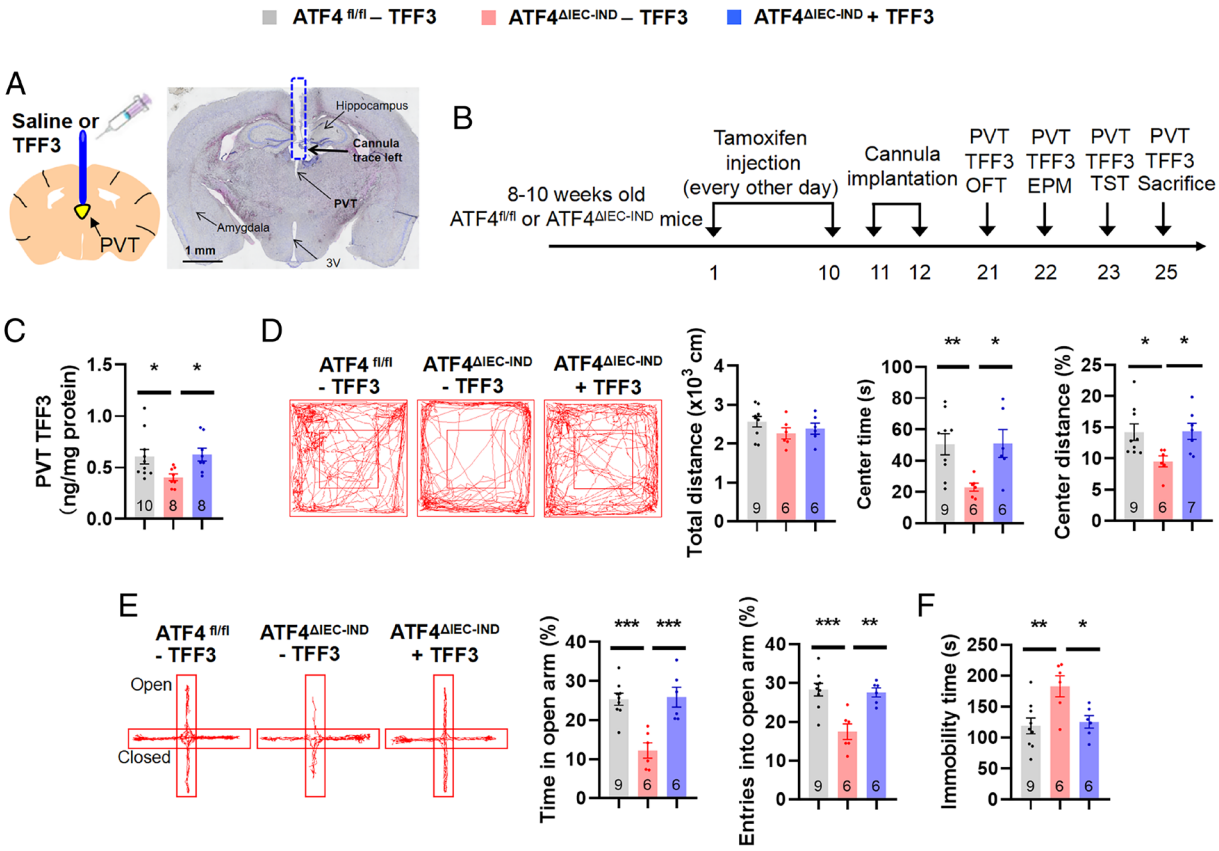

Fig. 5. PVT injection of TFF3 relieves intestinal ATF4 deletion caused behavioral alterations. (*A*) Schematic of PVT injection of TFF3 and representative image of Nissl staining to show the trace left by cannula in mice. (*B*) Timeline of the tamoxifen injection, cannula implantation, PVT injection of TFF3, and behavioral tests in ATF4$^{fl/fl}$ or ATF4$^{\triangle IEC\text{-}IND}$ mice. OFT, open-field test; EPM, elevated plus-maze test; TST, tail suspension test. (*C*) TFF3 levels in the PVT by ELISA ($F_{2,23}$ = 3.886; P = 0.0352; CV of ATF4$^{fl/fl}$: 36.90%, CV of ATF4$^{\triangle IEC\text{-}IND}$: 23.22%, CV of ATF4$^{\triangle IEC\text{-}IND}$ + TFF3: 28.05%). (*D*) Representative tracks of mice in OFT, travel distance ($F_{2,18}$ = 1.182; P = 0.3295), time spent in center ($F_{2,18}$ = 5.074; P = 0.0179), and percentage of distance in center area (Kruskal–Wallis test, P = 0.0182). (*E*) Representative tracks of mice in EPM, percentage of time spent in the open arms ($F_{2,18}$ = 14.37; P = 0.0002), and percentage of entries into the open arms ($F_{2,18}$ = 12.32; P = 0.0004). (*F*) Immobility time of TST ($F_{2,18}$ = 6.345; P = 0.0082). Studies were conducted using 12 to 14-wk-old male ATF4$^{fl/fl}$ or ATF4$^{\triangle IEC\text{-}IND}$ mice receiving PVT injection of saline (−TFF3) or TFF3 (+TFF3). Data are expressed as the mean ± SEM (the number of samples is indicated in the bar graph), with individual data points. Data were analyzed via one-way ANOVA or specific test marked in the data. *P < 0.05, **P < 0.01, ***P < 0.001.

TFF3 can act on brain regions to exhibit antidepressant-like effects. TFF3 increases c-Fos expression in the BLA via PI3K/AKT signaling, as well as in the PVN (58, 76), and acts in the hippocampal CA3 via the BDNF–ERK–CREB pathway (55). Our study did not find consistent changes in these regions, but the c-Fos expression in the PVT changed substantially in both strains of mice with intestinal epithelial ATF4 deletion. The PVT is an integral part of the emotional processing network that responds to arousal, reward, anxiety, depression, stress, and fear (51, 77–79). However, its specific role in regulating chronic stress and related behaviors has not been well elucidated. The PVT participates in stress-related behavioral regulation, but some results are discrepant and require further characterization (80). A recent study reported gut–PVT signals regulating anxiety (46), implying that the PVT can receive gut signals. Furthermore, the PVT can receive and send signals to other brain regions, such as the lateral hypothalamus, central nucleus of the amygdala, and bed nucleus of the stria terminalis, which are closely related to stress-induced behavioral alterations (79, 80). Hence, the PVT may send projections to stress-related brain areas to exert corresponding behavioral alterations.

It remains unknown in our study, how TFF3 activates PVT glutamatergic neurons. As mentioned above, TFF3 can activate BDNF–ERK–CREB signaling in the hippocampal CA3 region and PI3K/AKT signaling in the BLA (55, 58). How TFF3 activates these signals remains to be explored. Although TFF3 can bind to EGFR, CXCR4, and LONGO2 receptors (69, 81), specific cell surface receptors for TFF3 have not been identified. More in-depth work is needed in the future.

In addition, there are several questions remain unsolved in our studies. First, the relative role of inflammation in ATF4-deficient mice was uncertain, as the embryonic intestinal ATF4 knockout mice showed inflammatory phenotype, which is closely related to stress and anxiety/depression-related behaviors (21, 22). However, the effects of gut ATF4 on stress-related behavioral alterations were also observed in inducible intestinal ATF4 deletion mice, which were absent of intestinal inflammation, suggesting that inflammation was unlikely to be involved in this regulation. The relative role of inflammation in ATF4-deficient mice needs further investigation. Second, though the inducible ATF4-deficient mice showed decreased sucrose preference in SPT, we could not conclude that ATF4-deficient mice were anhedonic, since we did not exclude the possibility such as taste changes or caloric need (82). In addition, our study has the limitations that we could not be absolutely sure that the effects of ATF4 deficiency are mediated by TFF3 or PVT, as PVT injection of TFF3 in wild-type mice also exhibits beneficial behaviors and inhibition of PVT neurons exhibits stress-related behaviors. However, TFF3 is directly regulated by ATF4 and the PVT neural activity has corresponding changes after ATF4 deletion or chronic stress. Furthermore, supplement of TFF3 and activation of PVT neurons could relieve gut ATF4 deletion-induced behavioral alterations. We suspected that the role of ATF4 deletion in this regulation may be mediated by TFF3 and PVT neurons. The ATF4 overexpression model with

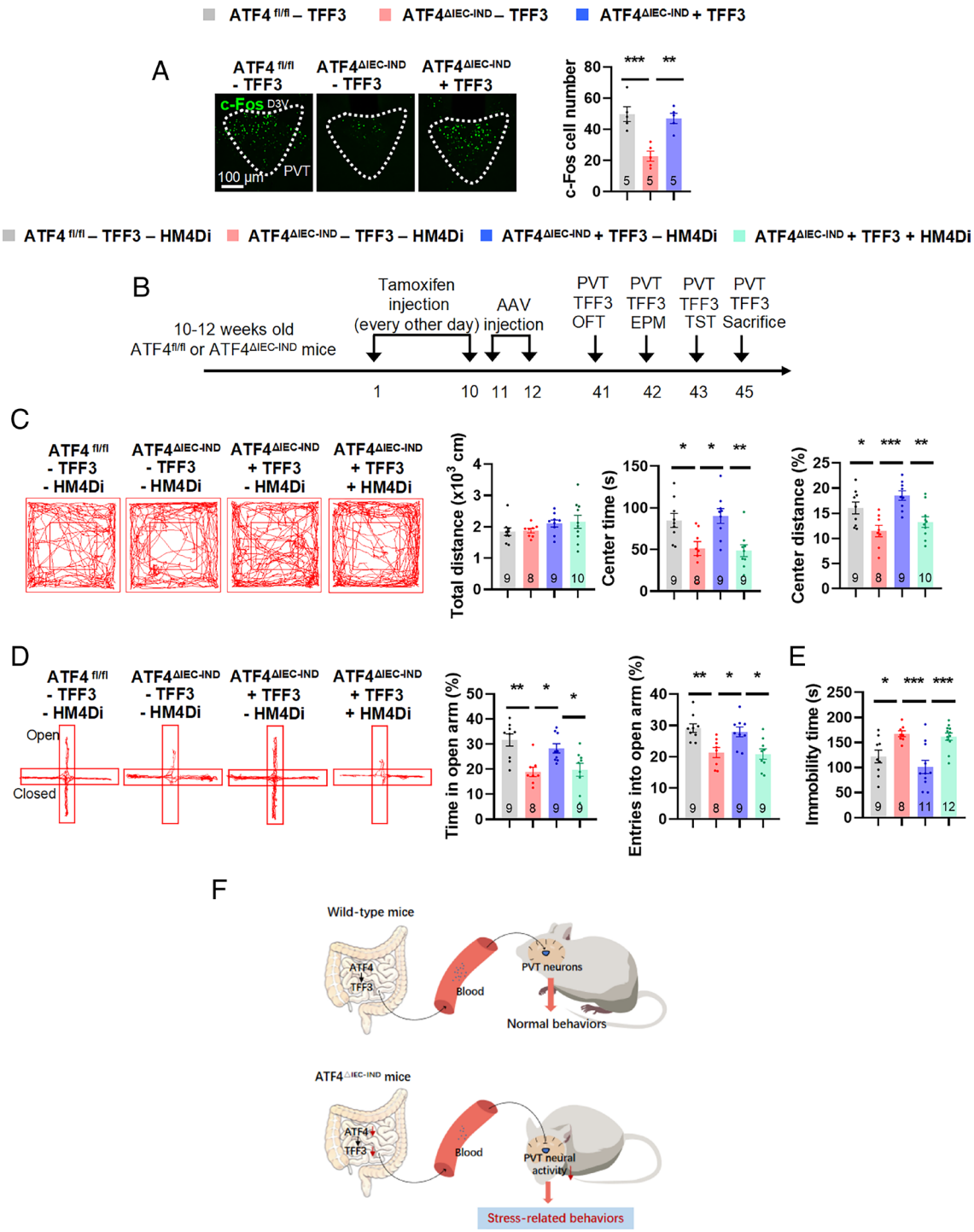

Fig. 6. Inhibition of PVT glutamatergic neurons blocks TFF3-induced beneficial effects in intestinal ATF4 knockout mice. (*A*) IF staining for c-Fos (green) in the PVT (*Left*) and quantification of c-Fos cell numbers (*Right*) ($F_{2,12}$ = 15.17; P = 0.0005); D3V, dorsal 3rd ventricle. (*B*) Timeline of the tamoxifen injection, TFF3 i.p. injection, and behavioral tests in ATF4$^{fl/fl}$ or ATF4$^{\triangle IEC\text{-}IND}$ mice. OFT, open-field test; EPM, elevated plus-maze test; TST, tail suspension test. (*C*) Representative tracks of mice in OFT, travel distance (Brown–Forsythe ANOVA test, $F^{*}_{3.000,21.48}$ = 1.289; P = 0.3035), time spent in center ($F_{3,31}$ = 7.131; P = 0.0009), and percentage of distance in center area ($F_{3,32}$ = 7.854; P = 0.0005). (*D*) Representative tracks of mice in EPM, percentage of time spent in the open arms ($F_{3,31}$ = 7.916; P = 0.0005), and percentage of entries into the open arms ($F_{3,31}$ = 7.815; P = 0.0005). (*E*) Immobility time of TST ($F_{3,36}$ = 9.359; P = 0.0001). (*F*) Summary diagram: Intestinal epithelial ATF4 regulated the expression of the gut-secreted peptide TFF3, which activated PVT glutamatergic neurons to induce antidepressant effects. Studies for *A* were conducted using 14 to 16-wk-old male ATF4$^{fl/fl}$ or ATF4$^{\triangle IEC\text{-}IND}$ mice receiving i.p. injection of saline (−TFF3) or TFF3 (+TFF3); studies for *B*–*E* were conducted using 12 to 14-wk-old male ATF4$^{fl/fl}$ or ATF4$^{\triangle IEC\text{-}IND}$ mice receiving AAVs expressing mCherry (−HM4Di) or HM4Di (+HM4Di), followed by CNO and TFF3 i.p. injection. Data are expressed as the mean ± SEM (the number of samples is indicated in the bar graph), with individual data points. Data were analyzed via one-way ANOVA or specific test marked in the data. *P < 0.05, **P < 0.01, ***P < 0.001.

TFF3 inhibitor and PVT neural inhibition may help to solve this problem in the future. In fact, we could also not exclude other mechanisms or signals that may mediate the gut ATF4 roles in stress-related behaviors, which require to be investigated in the following study.

In conclusion, this study demonstrated that colonic epithelial cell-specific ATF4 overexpression alleviated CRS-induced behaviors, whereas deletion of intestinal epithelial cell-specific ATF4 resulted in stress-related behaviors. Furthermore, gut ATF4 regulated TFF3

expression and changed TFF3 levels in the serum and PVT, thereby activating PVT glutamatergic neurons and ultimately exhibiting beneficial behavioral alterations. Our research identified ATF4 as a stress-responsive signal contributing to stress-related behaviors and described a TFF3-dependent pathway regulating stress-related behaviors. Moreover, a unique pathway of the gut–brain axis connecting intestinal epithelial cells with the PVT via peptide signaling has been characterized. Our research provides further evidence for the role of gut–brain signals in the regulation of stress-related behaviors and identifies possible targets for the pharmacological treatment of stress-related behavioral disorders.

Materials and Methods

Mice and Diets. All mice were of a C57BL/6J background. ATF4-floxed ($ATF4^{fl/fl}$), Villin-Cre, and Villin-CreER mice were obtained from The Jackson Laboratory (Bar Harbor, ME, USA) (33, 43). To generate embryonic intestine-specific ATF4 knockout ($ATF4^{\triangle IEC}$) mice, Villin-Cre mice were crossed with $ATF4^{fl/fl}$ mice. To generate inducible intestine-specific ATF4 knockout ($ATF4^{\triangle IEC\text{-}IND}$) mice, Villin-CreER mice were crossed with $ATF4^{fl/fl}$ mice. Tamoxifen (50 mg/kg; Sigma-Aldrich) suspended in corn oil (Sigma-Aldrich) was intraperitoneally (i.p.) injected into 8-wk-old male $ATF4^{fl/fl}$ or $ATF4^{\triangle IEC\text{-}IND}$ littermate mice every other day for 10 d to generate mice with adult-onset ATF4 deletion in the intestine. The behavioral tests or biochemical test was performed at least 10 d after the final injection of tamoxifen. Food intake and body weight were recorded daily. The mice were maintained under a 12-h/12-h light/dark cycle (lights on at 07:00/lights off at 19:00) and 22 to 25 °C, with ad libitum access to water and rodent standard chow diet before the experiments. Animal experiments were conducted in accordance with the guidelines of the Institutional Animal Care and Use Committee of Fudan University.

Ethic Statements. Animal research complied with all relevant ethnic regulations. These studies received ethical approval by the Institutional Animal Care and Use Committee of Fudan University.

Isolation of Intestinal Epithelial Cells. The epithelial cells of the intestines were extracted as described previously (33, 83). Briefly, mice were first killed, and intestines were collected and opened longitudinally and immediately washed with ice-cold PBS thoroughly. After that, four segments of the intestines were placed in 1.5 mM EDTA in Hank's balanced salt solution (HBSS) without calcium and magnesium and under gentle shaking for 10 min at 37 °C. The mucosa was incubated again with HBSS/EDTA for 10 min at 37 °C. Tissue fragments were removed, and cells recovered in the suspension were collected.

Colonic AAV Administration. To overexpress ATF4 in colon epithelial cells, Villin-Cre mice were fasted overnight and injected with 100 μL Cre-dependent AAVs, containing the ATF4 sequence and mCherry protein in the opposite orientation flanked by two inverted loxP sites (AAV2/9-EF1a-DIO–ATF4-mCherry; 1×10^{12} Pfu/mL) (84), or AAVs, containing only mCherry (AAV2/9-EF1a-DIO–mCherry; 1×10^{12} Pfu/mL), into the colon at a depth of 4 cm from the anus (85, 86). Next, the mice were held in an inverted vertical position for 5 min to ensure the distribution of the AAVs throughout the colon. The mice were allowed for recovery and AAV expression for 4 wk before the experiments.

Stereotaxic Surgery and Intracerebral Cannulation. Stereotaxic surgery and intracerebral cannulation were performed using a stereotaxic frame (Stoelting) (87, 88). Mouse body temperature was maintained using a heating pad. Ophthalmic ointment was applied to maintain eye lubrication. Before the surgery, male mice were i.p. injected with a combination of xylazine (10 mg/kg) anesthesia and ketamine (100 mg/kg) analgesia. A cannula was placed into the paraventricular thalamus (PVT; coordinates: ML: 0 mm, AP: −1.5 mm, DV: −3.1 mm from bregma), and two screws were placed at the lambdoid structure to aid in supporting the cannula in the skull with dental cement. The mice were allowed to recover from anesthesia on a heat blanket and were injected for 3 d with antibiotics (ceftriaxone sodium, 0.1 g/kg i.p.) to prevent infection. The mice were individually housed and allowed to recover for 7 to 10 d after the surgery.

Drugs and Treatment. For intracerebral injection of TFF3, recombined mouse TFF3 (Novoprotein) was freshly dissolved in sterile saline (1 ng/μL) (58). TFF3 or saline (1 μL) was injected into the PVT 30 min before the experiments. For TFF3 i.p. injection, TFF3 (0.1 mg/kg) or saline was injected at a volume of 10 mL/kg body weight 30 min before the experiments (55).

DREADDs. To activate PVT glutamatergic neurons using DREADDs, $ATF4^{fl/fl}$, $ATF4^{\triangle IEC\text{-}IND}$, or wild-type (WT) mice were stereotaxically injected with 200 nL AAVs including a CAMKIIα promoter encoding an excitatory DREADD GPCR (hM3Dq; AAV2/9-CAMKIIα–hM3Dq-mCherry, 4×10^{12} Pfu/mL) or only encoding mCherry (AAV2/9-CAMKIIα–mCherry, 4×10^{12} Pfu/mL) as a control into the PVT.

To inhibit PVT glutamatergic neurons using DREADDs, we injected the PVT of WT, $ATF4^{fl/fl}$, or $ATF4^{\triangle IEC\text{-}IND}$ mice with AAVs including a CAMKIIα promoter expressing inhibitory DREADD GPCR (hM4Di; AAV2/9-CAMKIIα–hM4Di-mCherry, 4×10^{12} Pfu/mL), or mCherry (AAV2/9- CAMKIIα–mCherry, 4×10^{12} Pfu/mL).

Four weeks after AAV delivery, all mice received i.p. injections of clozapine N-oxide (CNO; MedChemExpress) at 1 mg/kg of body weight for hM3Dq activation or at 3 mg/kg of body weight for hM4Di silencing.

CRS Protocol. The experiments were performed after acclimatizing the mice to the experimental environment for a week. Male WT mice (8 to 11 wk old) were divided into two weight-matched groups, the control and CRS groups. CRS mice were exposed to 3-h restraint (13:00 to 16:00) daily for 21 d in a 50-mL tube with holes that permitted breathing while restricting limb movements (41). The mice had no access to food and water during restraint. At the same time, control mice were placed in their home cages without food or water. After restraint, the mice were returned to home cages and given food and water ad libitum. Before subsequent experiments, mice were allowed to rest 1 d after CRS to exclude acute stress effects (52).

Behavioral Assays. All behavioral tests were performed during the afternoon. All animals were brought into the experimental room 1 h before the start of behavioral tests and remained in this room throughout the test. Mice with DREADDs were injected with CNO 30 min before the tests (89). For TFF3 i.p. or intracerebral injections, mice were injected with TFF3 or saline 30 min before the behavioral tests.

OFT. Mice were placed in the center of a white plastic open-field arena (50 cm × 50 cm × 50 cm) in a brightly lit room and allowed to explore freely for 10 min (90). A video camera positioned directly above the arena was used to track animal movements, recorded on a computer with LabState (AniLab) to determine the total distance and the amount of time spent in the center of the chamber compared to the edges. The OFT is commonly used for assessing exploratory behavior and the general activity of animals. The area was cleaned with 75% ethanol after each test to remove olfactory cues.

EPM. The EPM consisted of a central platform (5×5 cm^2), two closed arms with walls, and two opposing open arms without walls (25 cm × 5 cm). The maze was placed 60 cm above the floor. A mouse was placed on the central platform facing an open arm and was allowed to explore the maze for 5 min (90). The time spent in the open arms and the number of entries into the open arms were analyzed using LabState. The area was cleaned between tests using 75% ethanol.

TST. Mice were individually suspended about 50 cm above the surface of a table using adhesive tape that was placed roughly 1 cm from the tip of the tail. The mice tails were passed through a small plastic cylinder to avoid tail climbing. Each mouse was tested only once for 6 min (91). The test was videotaped from the side, and the immobility time of the animal was measured in the last 5 min. Mice were considered immobile without initiated movements, excluding passive swaying. Video tracking data were analyzed using LabState software to extract the immobility time.

FST. The FST was conducted in a cylindrical container (15 cm diameter, 25 cm height) that was filled with water (15 to 18 cm depth) at a temperature of 23 ± 1 °C as previously described (92). The mice were subjected to FST for 6 min. Immobility was defined as time when mice remained floating or motionless with only movements necessary for keeping balance in the water. The results were shown as the amount of time (in seconds) that the mice spent immobile during the last 4 min of the test.

SPT. Male mice were housed singly for 2 d and then habituated with one bottle of water and another bottle with 1% sucrose solution for 2 d. The left/right location of the bottles was switched every day to prevent a possible effect of behavior. Before the test, the mice were water-deprived for 24 h, then given access to two bottles of water or sucrose. The first 1 h of sucrose intake over total water and sucrose intake was used for calculation. Sucrose preference was measured as the percentage of sucrose intake over total water and sucrose intake.

Cell Culture and Treatments. The human colon epithelial cell line CCD-841 was purchased from the Cell Bank of Shanghai Institute of Cell Biology, Chinese Academy of Sciences. Recombinant adenoviruses used for the expression of ATF4 (Ad-ATF4) and dominant-negative ATF4 mutant (Ad-DN-ATF4) were generated using the AdEsay Adenoviral Vector System (pAdEasy-EF1a-MCS-CMV-EGFP vector; Qbiogene) (93). CCD-841 cells were infected with Ad-GFP, Ad-ATF4, or Ad-DN-ATF4 at a dose of 5×10^8 Pfu/well in 12-well plates for 48 h.

Luciferase Assay. pGL3-TFF3 promoter (−2,000 to 0 bp) was generated by BioSune Corporation (Shanghai, China). CCD-841 cells were infected with Ad-ATF4 for 24 h and then cotransfected with the internal control vector pRL Renilla and pGL3-TFF3 using Lipofectamine 2000. Firefly and Renilla luciferase activities were assayed using Dual-Glo Luciferase Assay System (Promega).

Isolation and Treatment of Primary Thalamic Neurons. Primary cultures of thalamic neurons were prepared and cultured as previously described (94). On day 10, primary cultured neurons were treated with different concentrations of TFF3. Cells were collected 30 min after treatment for mRNA extraction and 60 min after treatment for IF staining.

TFF3 Level Measurements. TFF3 levels in the serum, gut, cerebrospinal fluid, and PVT of mice were measured using Mouse TFF3 ELISA kit (E-EL-M1200c, Vazyme Biotech, Nanjing, China) according to the manufacturer's recommendations. The threshold of the TFF3 Elisa kit was 78.13 to 5,000 pg/mL and the intra- and inter-assay coefficients of variation were less than 10 as provided in the specification of the ELISA Kit.

Hematoxylin and Eosin (H&E) Staining and Nissl Staining. Colon tissue was fixed in 4% paraformaldehyde (PFA) overnight. Tissues were embedded in paraffin and cut into 8-μm slices. After deparaffinization and rehydration, sections were stained with H&E. The stained sections were analyzed to determine the degree of inflammation and tissue damage.

Fixed brain slices were stained with Nissl Staining Solution (Beyotime Biotechnology) according to the specification.

IF Staining. Mice were transcardially perfused with saline followed by phosphate-buffered saline (PBS) containing 4% PFA. Mouse brains were dissected and fixed overnight at 4 °C in 4% PFA, followed by cryoprotection in PBS containing 20% and 30% sucrose at 4 °C. Free-floating sections (25 μm) were prepared with a cryostat. Slices were blocked for 1 h at room temperature in PBST (0.3% Triton X-100) with 5% normal donkey serum, followed by incubation with primary antibodies at 4 °C overnight and secondary antibodies at room temperature for 2 h. Primary antibodies used in IF experiments included anti-CAMKIIα (1:1,000, #50049) and anti-c-Fos (1:1,000, #2250; both Cell Signaling Technology).

Western Blot Analysis. Tissues were homogenized in ice-cold lysis buffer (50 mM Tris HCl, pH 7.5, 0.5% Nonidet P-40, 150 mM NaCl, 2 mM EGTA, 1 mM Na_3VO_4, 100 mM NaF, 10 mM $Na_4P_2O_7$, 1 mM phenylmethylsulfonyl fluoride, 10 μg/mL aprotinin, 10 μg/mL leupeptin). Tissue extracts were then immunoblotted with anti-ATF4 (1:1,000, #11815, Cell Signaling Technology) and anti-β-actin (1:5,000, Sigma-Aldrich) primary antibodies. The full gels of the western blots together with molecular weight markers are shown in *SI Appendix*, Fig. S18.

RNA Sequencing (RNA-Seq) and Data Analysis. Total RNA from ileum epithelial cells was extracted using TRIzol (Invitrogen). For RNA sequencing library synthesis, 2.5 μg total RNA was first depleted of rRNA using the Ribo-Zero rRNA Magnetic Kit (Plant Seed/Root kit, Epicentre). Sequencing libraries were generated using NEBNext® UltraTM RNA Library Prep Kit for Illumina® (NEB, USA) following manufacturer's recommendations. Sequencing was then performed on an Illumina HiSeq 2500 platform, and 150 bp paired-end reads were generated. Raw data (raw reads) of fastq format and clean reads were processed as described previously (33). Differential expression analysis of the genes from two groups was performed by using the DESeq2 R package. Genes with P-value <0.05, or fold change >1.5 or <0.5, were chosen for further analysis by setting parameters on the Majorbio Cloud Platform (Shanghai Majorbio Bio-pharm Technology). In order to identify possible secreted proteins derived from the gut that may act on the brain, we crossanalyzed our data with previously published data of annotated as gut-secreted peptides as well as which have correlation on brain functions (54). Finally, we ranked the results based on the significance of the correlation.

RNA Isolation and RT-PCR. RNA was extracted using TRIzol reagent (Invitrogen). mRNA was reverse-transcribed using a High-Capacity cDNA Reverse Transcription Kit (Thermo Scientific) and subjected to quantitative real-time PCR analysis using SYBR Green I Master Mix reagent on an ABI 7900 system (Applied Biosystems). The primer sequences used in this study are described in *SI Appendix*, Table S1.

Statistical Analysis and Reproducibility. Statistical analyses were performed using GraphPad Prism, version 8.0 (GraphPad Software). All values were presented as the mean ± SEM. Two groups were compared using the two-tailed unpaired Student's t test. For experiments involving multiple comparisons, data were analyzed using one-way ANOVA or two-way ANOVA, followed by Tukey's or Dunnett's multiple comparisons test. For the data that did not pass the normality of distribution or the equal variances test, we analyzed the results using other statistical methods (89). For data of the two groups with unequal variances, two-tailed t tests with the Welch's correction were used. For the two groups with nonnormally distributed data, Mann–Whitney U tests were used. For the three or more groups with nonnormally distributed data, the Kruskal–Wallis test followed by post hoc multiple comparison tests was performed. For normally distributed data of three or more groups with unequal variances, Brown–Forsythe ANOVA test was used. Individual data points were shown for each histogram to reflect data variability, and the number of animals per group was shown in the graph. Statistical significance levels were defined as $*P < 0.05$, $**P < 0.01$, $***P < 0.001$, and $****P < 0.0001$. The normality of distribution, equal variances, t/F values, and degrees of freedom of the all the data are shown in *SI Appendix*, Table S2.

Data, Materials, and Software Availability. The resource data of RNA-Seq have been deposited in NCBI Sequence Read Archive with the accession number PRJNA838867 (53). All other study data are included in the article and/or *SI Appendix*.

ACKNOWLEDGMENTS. This work was supported by the National Natural Science Foundation (grants 31830044, 91957207, 81870592, 82270905, 81970742, 82000764, 82170868, and 81970731) and the National Key R&D Program of China (grant 2018YFA0800600).

Author affiliations: [a]Zhongshan Hospital, State Key Laboratory of Medical Neurobiology, Institute for Translational Brain Research, Minister of Education Frontiers Center for Brain Science, Fudan University, Shanghai 200032, China; [b]Chinese Academy of Sciences Key Laboratory of Nutrition, Metabolism and Food Safety, Innovation Center for Intervention of Chronic Disease and Promotion of Health, Shanghai Institute of Nutrition and Health, University of Chinese Academy of Sciences, Chinese Academy of Sciences, Shanghai 200031, China; and [c]Center for Inflammatory Bowel Disease Research, The Shanghai Tenth People's Hospital, Tongji University School of Medicine, Shanghai 200072, China

1. E. R. de Kloet, M. Joels, F. Holsboer, Stress and the brain: From adaptation to disease. *Nat. Rev. Neurosci.* **6**, 463–475 (2005).
2. G. S. Malhi, J. J. Mann, Depression. *Lancet* **392**, 2299–2312 (2018).
3. A. J. Ferrari *et al.*, Burden of depressive disorders by country, sex, age, and year: Findings from the global burden of disease study 2010. *PLoS Med.* **10**, e1001547 (2013).
4. D. A. Pizzagalli, Depression, stress, and anhedonia: Toward a synthesis and integrated model. *Annu. Rev. Clin. Psychol.* **10**, 393–423 (2014).
5. S. Moussavi *et al.*, Depression, chronic diseases, and decrements in health: Results from the World Health Surveys. *Lancet* **370**, 851–858 (2007).
6. J. S. Seo *et al.*, Cellular and molecular basis for stress-induced depression. *Mol. Psychiatry* **22**, 1440–1447 (2017).
7. R. B. Price, R. Duman, Neuroplasticity in cognitive and psychological mechanisms of depression: An integrative model. *Mol. Psychiatry* **25**, 530–543 (2020).
8. A. Ribeiro, J. P. Ribeiro, O. von Doellinger, Depression and psychodynamic psychotherapy. *Braz J. Psychiatry* **40**, 105–109 (2018).
9. S. Liu *et al.*, Fat mass and obesity-associated protein regulates RNA methylation associated with depression-like behavior in mice. *Nat. Commun.* **12**, 6937 (2021).
10. C. Kraus, E. Castren, S. Kasper, R. Lanzenberger, Serotonin and neuroplasticity–Links between molecular, functional and structural pathophysiology in depression. *Neurosci. Biobehav. Rev.* **77**, 317–326 (2017).
11. H. K. Manji, W. C. Drevets, D. S. Charney, The cellular neurobiology of depression. *Nat. Med.* **7**, 541–547 (2001).
12. C. Andrade, Relative efficacy and acceptability of antidepressant drugs in adults with major depressive disorder: Commentary on a network meta-analysis. *J. Clin. Psychiatry* **79**, 18f12254 (2018).
13. P. C. Casarotto *et al.*, Antidepressant drugs act by directly binding to TRKB neurotrophin receptors. *Cell* **184**, 1299–1313.e19 (2021).

14. J. Duan *et al.*, Characterization of gut microbiome in mice model of depression with divergent response to escitalopram treatment. *Transl. Psychiatry* **11**, 303 (2021).
15. R. Dantzer, J. C. O'Connor, G. G. Freund, R. W. Johnson, K. W. Kelley, From inflammation to sickness and depression: When the immune system subjugates the brain. *Nat. Rev. Neurosci.* **9**, 46–56 (2008).
16. G. Winter, R. A. Hart, R. P. G. Charlesworth, C. F. Sharpley, Gut microbiome and depression: What we know and what we need to know. *Rev. Neurosci.* **29**, 629–643 (2018).
17. B. R. Stevens *et al.*, Increased human intestinal barrier permeability plasma biomarkers zonulin and FABP2 correlated with plasma LPS and altered gut microbiome in anxiety or depression. *Gut* **67**, 1555–1557 (2018).
18. Y. Milaneschi, W. K. Simmons, E. F. C. van Rossum, B. W. Penninx, Depression and obesity: Evidence of shared biological mechanisms. *Mol. Psychiatry* **24**, 18–33 (2019).
19. Z. Yang *et al.*, Updated review of research on the gut microbiota and their relation to depression in animals and human beings. *Mol. Psychiatry* **25**, 2759–2772 (2020).
20. K. M. Sawyer, P. A. Zunszain, P. Dazzan, C. M. Pariante, Intergenerational transmission of depression: Clinical observations and molecular mechanisms. *Mol. Psychiatry* **24**, 1157–1177 (2019).
21. M. I. Pinto-Sanchez *et al.*, Probiotic Bifidobacterium longum NCC3001 reduces depression scores and alters brain activity: A pilot study in patients with irritable bowel syndrome. *Gastroenterology* **153**, 448–459.e8 (2017).
22. B. Barberio, M. Zamani, C. J. Black, E. V. Savarino, A. C. Ford, Prevalence of symptoms of anxiety and depression in patients with inflammatory bowel disease: A systematic review and meta-analysis. *Lancet Gastroenterol. Hepatol.* **6**, 359–370 (2021).
23. G. Fond *et al.*, Anxiety and depression comorbidities in irritable bowel syndrome (IBS): A systematic review and meta-analysis. *Eur. Arch. Psychiatry Clin. Neurosci.* **264**, 651–660 (2014).
24. J. Luo, Z. Xu, R. Noordam, D. van Heemst, R. Li-Gao, Depression and inflammatory bowel disease: A bidirectional two-sample Mendelian randomization study. *J. Crohns Colitis* **16**, 633–642 (2022).
25. M. Rao, M. D. Gershon, The bowel and beyond: The enteric nervous system in neurological disorders. *Nat. Rev. Gastroenterol. Hepatol.* **13**, 517–528 (2016).
26. L. J. Sun, J. N. Li, Y. Z. Nie, Gut hormones in microbiota-gut-brain cross-talk. *Chin Med. J. (Engl)* **133**, 826–833 (2020).
27. R. Coccurello, Anhedonia in depression symptomatology: Appetite dysregulation and defective brain reward processing. *Behav. Brain Res.* **372**, 112041 (2019).
28. M. Valles-Colomer *et al.*, The neuroactive potential of the human gut microbiota in quality of life and depression. *Nat. Microbiol.* **4**, 623–632 (2019).
29. W. Marx *et al.*, Diet and depression: Exploring the biological mechanisms of action. *Mol. Psychiatry* **26**, 134–150 (2021).
30. D. K. L. Tsang *et al.*, A single cell survey of the microbial impacts on the mouse small intestinal epithelium. *Gut Microbes* **14**, 2108281 (2022).
31. T. Hai, M. G. Hartman, The molecular biology and nomenclature of the activating transcription factor/cAMP responsive element binding family of transcription factors: activating transcription factor proteins and homeostasis. *Gene* **273**, 1–11 (2001).
32. T. Hai, T. Curran, Cross-family dimerization of transcription factors Fos/Jun and ATF/CREB alters DNA binding specificity. *Proc. Natl. Acad. Sci. U.S.A.* **88**, 3720–3724 (1991).
33. X. Hu *et al.*, ATF4 deficiency promotes intestinal inflammation in mice by reducing uptake of glutamine and expression of antimicrobial peptides. *Gastroenterology* **156**, 1098–1111 (2019).
34. I. M. N. Wortel, L. T. van der Meer, M. S. Kilberg, F. N. van Leeuwen, Surviving stress: Modulation of ATF4-mediated stress responses in normal and malignant cells. *Trends Endocrinol. Metabolism* **28**, 794–806 (2017).
35. C. Wang *et al.*, ATF4 regulates lipid metabolism and thermogenesis. *Cell Res.* **20**, 174–184 (2010).
36. H. P. Harding *et al.*, An integrated stress response regulates amino acid metabolism and resistance to oxidative stress. *Mol. Cell* **11**, 619–633 (2003).
37. H. Malhi, R. J. Kaufman, Endoplasmic reticulum stress in liver disease. *J. Hepatol.* **54**, 795–809 (2011).
38. N. Wei, L. Q. Zhu, D. Liu, ATF4: A novel potential therapeutic target for Alzheimer's disease. *Mol. Neurobiol.* **52**, 1765–1770 (2015).
39. A. Shah, J. Chao, C. Legido-Quigley, R. C. Chang, Oxyresveratrol exerts ATF4- and Grp78-mediated neuroprotection against endoplasmic reticulum stress in experimental Parkinson's disease. *Nutr. Neurosci.* **24**, 181–196 (2021).
40. B. S. McEwen, J. H. Morrison, The brain on stress: Vulnerability and plasticity of the prefrontal cortex over the life course. *Neuron* **79**, 16–29 (2013).
41. Y. Wang *et al.*, Sperm microRNAs confer depression susceptibility to offspring. *Sci. Adv.* **7**, eabd7605 (2021).
42. C. Jousse *et al.*, TRB3 inhibits the transcriptional activation of stress-regulated genes by a negative feedback on the ATF4 pathway. *J. Biol. Chem.* **282**, 15851–15861 (2007).
43. F. el Marjou *et al.*, Tissue-specific and inducible Cre-mediated recombination in the gut epithelium. *Genesis* **39**, 186–193 (2004).
44. S. Sabui *et al.*, Tamoxifen-induced, intestinal-specific deletion of Slc5a6 in adult mice leads to spontaneous inflammation: Involvement of NF-kappaB, NLRP3, and gut microbiota. *Am. J. Physiol. Gastrointest. Liver Physiol.* **317**, G518–G530 (2019).
45. J. M. Peirce, K. Alvina, The role of inflammation and the gut microbiome in depression and anxiety. *J. Neurosci. Res.* **97**, 1223–1241 (2019).
46. B. D. Needham *et al.*, A gut-derived metabolite alters brain activity and anxiety behaviour in mice. *Nature* **602**, 647–653 (2022).
47. T. Curran, J. I. Morgan, Fos: An immediate-early transcription factor in neurons. *J. Neurobiol.* **26**, 403–412 (1995).
48. S. A. Rowson, K. E. Pleil, Influences of stress and sex on the paraventricular thalamus: Implications for motivated behavior. *Front. Behav. Neurosci.* **15**, 636203 (2021).
49. T. M. Kato *et al.*, Presynaptic dysregulation of the paraventricular thalamic nucleus causes depression-like behavior. *Sci. Rep.* **9**, 16506 (2019).
50. T. Kasahara *et al.*, Depression-like episodes in mice harboring mtDNA deletions in paraventricular thalamus. *Mol. Psychiatry* **21**, 39–48 (2016).
51. S. Ren *et al.*, The paraventricular thalamus is a critical thalamic area for wakefulness. *Science* **362**, 429–434 (2018).
52. X. Zhu *et al.*, Distinct thalamocortical circuits underlie allodynia induced by tissue injury and by depression-like states. *Nat. Neurosci.* **24**, 542–553 (2021).
53. F. Yuan *et al.*, *Mus musculus* raw sequence reads. *NCBI Sequence Read Archive*. https://www.ncbi.nlm.nih.gov/bioproject/PRJNA838867/. Deposited 26 May 2022.
54. M. M. Seldin *et al.*, A strategy for discovery of endocrine interactions with application to whole-body metabolism. *Cell Metabol.* **27**, 1138–1155.e6 (2018).
55. J. Li *et al.*, Neuropeptide trefoil factor 3 reverses depressive-like behaviors by activation of BDNF-ERK-CREB signaling in olfactory bulbectomized rats. *Int. J. Mol. Sci.* **16**, 28386–28400 (2015).
56. B. A. Karpinski, G. D. Morle, J. Huggenvik, M. D. Uhler, J. M. Leiden, Molecular cloning of human CREB-2: An ATF/CREB transcription factor that can negatively regulate transcription from the cAMP response element. *Proc. Natl. Acad. Sci. U.S.A.* **89**, 4820–4824 (1992).
57. W. Jagla, A. Wiede, K. Dietzmann, K. Rutkowski, W. Hoffmann, Co-localization of TFF3 peptide and oxytocin in the human hypothalamus. *FASEB J.* **14**, 1126–1131 (2000).
58. H. S. Shi *et al.*, PI3K/Akt signaling pathway in the basolateral amygdala mediates the rapid antidepressant-like effects of trefoil factor 3. *Neuropsychopharmacology* **37**, 2671–2683 (2012).
59. K. G. Margolis, J. F. Cryan, E. A. Mayer, The microbiota-gut-brain axis: From motility to mood. *Gastroenterology* **160**, 1486–1501 (2021).
60. X. Liu *et al.*, High-fiber diet mitigates maternal obesity-induced cognitive and social dysfunction in the offspring via gut-brain axis. *Cell Metabol.* **33**, 923–938.e6 (2021).
61. J. Wang *et al.*, MicroRNA-214-3p: A link between autophagy and endothelial cell dysfunction in atherosclerosis. *Acta Physiol. (Oxf)* **222** (2018), https://doi.org/10.1111/apha.12973.
62. X. Wang *et al.*, miR-214 targets ATF4 to inhibit bone formation. *Nat. Med.* **19**, 93–100 (2013).
63. A. S. Krall *et al.*, Asparagine couples mitochondrial respiration to ATF4 activity and tumor growth. *Cell Metabol.* **33**, 1013–1026.e6 (2021).
64. M. Nagasawa, T. Murakami, S. Tomonaga, M. Furuse, The impact of chronic imipramine treatment on amino acid concentrations in the hippocampus of mice. *Nutr. Neurosci.* **15**, 26–33 (2012).
65. X. J. Liu *et al.*, Urinary metabonomic study using a CUMS rat model of depression. *Magn. Reson. Chem.* **50**, 187–192 (2012).
66. G. Lach, H. Schellekens, T. G. Dinan, J. F. Cryan, Anxiety, depression, and the microbiome: A role for gut peptides. *Neurotherapeutics* **15**, 36–59 (2018).
67. T. Pelaseyed *et al.*, The mucus and mucins of the goblet cells and enterocytes provide the first defense line of the gastrointestinal tract and interact with the immune system. *Immunol. Rev.* **260**, 8–20 (2014).
68. G. X. Jiang *et al.*, IL-6/STAT3/TFF3 signaling regulates human biliary epithelial cell migration and wound healing in vitro. *Mol. Biol. Rep.* **37**, 3813–3818 (2010).
69. N. M. Belle *et al.*, TFF3 interacts with LINGO2 to regulate EGFR activation for protection against colitis and gastrointestinal helminths. *Nat. Commun.* **10**, 4408 (2019).
70. K. Seselja *et al.*, Effect of Tff3 deficiency and ER stress in the liver. *Int. J. Mol. Sci.* **20**, 4389 (2019).
71. H. Ge *et al.*, Trefoil factor 3 (TFF3) is regulated by food intake, improves glucose tolerance and induces mucinous metaplasia. *PLoS One* **10**, e0126924 (2015).
72. J. Qin *et al.*, Enhanced antidepressant-like effects of the macromolecule trefoil factor 3 by loading into negatively charged liposomes. *Int. J. Nanomedicine* **9**, 5247–5257 (2014).
73. C. Fulling, T. G. Dinan, J. F. Cryan, Gut microbe to brain signaling: What happens in vagus. *Neuron* **101**, 998–1002 (2019).
74. N. Goldstein *et al.*, Hypothalamic detection of macronutrients via multiple gut-brain pathways. *Cell Metabol.* **33**, 676–687.e5 (2021).
75. B. Kim *et al.*, Response of the microbiome-gut-brain axis in Drosophila to amino acid deficit. *Nature* **593**, 570–574 (2021).
76. A. Derbyshire, M. Ludwig, TFF3 induced Fos protein expression in the magnocellular oxytocin neurons of the hypothalamus. *Peptides* **25**, 833–838 (2004).
77. M. A. Penzo *et al.*, The paraventricular thalamus controls a central amygdala fear circuit. *Nature* **519**, 455–459 (2015).
78. C. K. Lafferty, A. K. Yang, J. A. Mendoza, J. P. Britt, Nucleus accumbens cell type- and input-specific suppression of unproductive reward seeking. *Cell Rep.* **30**, 3729–3742.e3 (2020).
79. G. J. Kirouac, The Paraventricular nucleus of the thalamus as an integrating and relay node in the brain anxiety network. *Front. Behav. Neurosci.* **15**, 627633 (2021).
80. J. R. Barson, N. R. Mack, W. J. Gao, The paraventricular nucleus of the thalamus is an important node in the emotional processing network. *Front. Behav. Neurosci.* **14**, 598469 (2020).
81. H. Y. Cui *et al.*, CD147 receptor is essential for TFF3-mediated signaling regulating colorectal cancer progression. *Signal Transduct. Target. Ther.* **6**, 268 (2021).
82. H. E. Tan *et al.*, The gut-brain axis mediates sugar preference. *Nature* **580**, 511–516 (2020).
83. T. Hashimoto *et al.*, ACE2 links amino acid malnutrition to microbial ecology and intestinal inflammation. *Nature* **487**, 477–481 (2012).
84. F. Yuan *et al.*, Activation of GCN2/ATF4 signals in amygdalar PKC-delta neurons promotes WAT browning under leucine deprivation. *Nat. Commun.* **11**, 2847 (2020).
85. X. Zheng *et al.*, Adeno-associated virus-mediated colonic secretory expression of HMGB1 A box attenuates experimental colitis in mice. *J. Gene Med.* **18**, 261–272 (2016).
86. J. He *et al.*, Fbxw7 increases CCL2/7 in CX3CR1hi macrophages to promote intestinal inflammation. *J. Clin. Invest.* **129**, 3877–3893 (2019).
87. A. Cetin, S. Komai, M. Eliava, P. H. Seeburg, P. Osten, Stereotaxic gene delivery in the rodent brain. *Nat. Protoc.* **1**, 3166–3173 (2006).
88. T. Landry *et al.*, Central α-Klotho suppresses NPY/AgRP neuron activity and regulates metabolism in mice. *Diabetes* **69**, 1368–1381 (2020).
89. X. Fang *et al.*, Chronic unpredictable stress induces depression-related behaviors by suppressing AgRP neuron activity. *Mol. Psychiatry* **26**, 2299–2315 (2021).
90. K. Q. Fan *et al.*, Stress-induced metabolic disorder in peripheral CD4(+) T cells leads to anxiety-like behavior. *Cell* **179**, 864–879 e819 (2019).
91. W. Zhou *et al.*, A neural circuit for comorbid depressive symptoms in chronic pain. *Nat. Neurosci.* **22**, 1649–1658 (2019).
92. Y. Yang *et al.*, Ketamine blocks bursting in the lateral habenula to rapidly relieve depression. *Nature* **554**, 317–322 (2018).
93. Q. Zhang *et al.*, Central activating transcription factor 4 (ATF4) regulates hepatic insulin resistance in mice via S6K1 signaling and the vagus nerve. *Diabetes* **62**, 2230–2239 (2013).
94. F. Paraskevopoulou, M. A. Herman, C. Rosenmund, Glutamatergic innervation onto striatal neurons potentiates GABAergic synaptic output. *J. Neurosci.* **39**, 4448–4460 (2019).